The dynamics of the Mississippi River plume: Impact of topography, wind and offshore forcing on the fate of plume waters

R. V. Schiller,[1] V. H. Kourafalou,[1] P. Hogan,[2] and N. D. Walker[3]

Received 13 December 2010; revised 1 March 2011; accepted 16 March 2011; published 30 June 2011.

[1] High-resolution numerical simulations of the northern Gulf of Mexico region using the Hybrid Coordinate Ocean Model (HYCOM) were employed to investigate the dynamical processes controlling the fate of the Mississippi River plume, in particular the conditions that favor cross-marginal transport. The study focuses on the effects of topography, wind-driven and eddy-driven circulation on the offshore removal of plume waters. A realistically forced simulation (nested in a data-assimilative regional Gulf of Mexico HYCOM model) reveals that the offshore removal is a frequent plume pathway. Eastward wind-driven currents promote large freshwater transport toward the shelf break and the DeSoto Canyon, where eddies with diameters ranging from 50 to 130 km interact with the buoyant plume and effectively entrain the riverine waters. Our estimates show that the offshore removal by eddies can be as large as the wind-driven shelf transport. The proximity of eddies to the shelf break is a sufficient condition for offshore removal, and shelf-to-offshore interaction is facilitated by the steep bottom topography near the delta. Strong eddy-plume interactions were observed when the Loop Current System impinged against the shelf break, causing the formation of coherent, narrow low-salinity bands that extended toward the gulf interior. The offshore pathways depend on the position of the eddies near the shelf edge, their life span and the formation of eddy pairs that generate coherent cross-shelf flows. This study elucidates the dynamics that initiate a unique cross-marginal removal mechanism of riverine low-salinity, nutrient-rich waters, allowing their export along connectivity pathways, induced by a large-scale current system.

Citation: Schiller, R. V., V. H. Kourafalou, P. Hogan, and N. D. Walker (2011), The dynamics of the Mississippi River plume: Impact of topography, wind and offshore forcing on the fate of plume waters, *J. Geophys. Res.*, *116*, C06029, doi:10.1029/2010JC006883.

1. Introduction

[2] The Mississippi River (MR, Figure 1a) is the major source of freshwater, sediments and nutrients for the Gulf of Mexico (GoM). Draining 41% of the continental United States, it is the largest river in North America, ranks as the eighth largest worldwide in terms of discharge (mean $1.35 \pm 0.2 \times 10^4$ m^3 s^{-1} [*Hu et al.*, 2005]) and transports about 210 million tons of sediment to the GoM annually [*Milliman and Meade*, 1983]. The MR delivers highly productive waters that, together with other local rivers, fuel important fishery activities on the Louisiana-Texas shelf that yield approximately 28% of the total U.S. catch [*Rabalais et al.*, 1991]. At the same time, the nutrient-rich, riverine waters are responsible for the recurrent summertime hypoxia (oxygen concentration <2 mg l^{-1}) in bottom waters of the mid and inner shelf west of the MR delta [*Rabalais et al.*, 1991, 2002, 2007]. Understanding the processes controlling the transport and dispersion of the MR waters is important for ecosystem management and water quality purposes in the northern Gulf of Mexico (NGoM) region. The goal of this study is to explore the dynamic processes controlling the transport and fate of MR waters. In particular, we seek to determine the relative impact of the shelf wind-driven circulation and the offshore eddy-driven circulation on the evolution of the MR plume and the offshore removal of riverine waters.

[3] Approximately 70% of the MR flow enters the NGoM through the bird foot delta, where riverine waters exit through several passes, the largest of which are the Southwest Pass, South Pass and Pass a Loutre. The remaining 30% of the flow is discharged into the GoM by the Atchafalaya River further west [*Walker et al.*, 1994]. Mixing and spreading of the MR plume on the shelf are controlled by a variety of factors. The circulation in the NGoM inner continental shelf is primarily wind driven [*Cochrane and Kelly*, 1986;

[1]Rosenstiel School of Marine and Atmospheric Science, University of Miami, Miami, Florida, USA.
[2]Naval Research Laboratory, Stennis Space Center, Mississippi, USA.
[3]Department of Oceanography and Coastal Sciences, Louisiana State University, Baton Rouge, Louisiana, USA.

Copyright 2011 by the American Geophysical Union.
0148-0227/11/2010JC006883

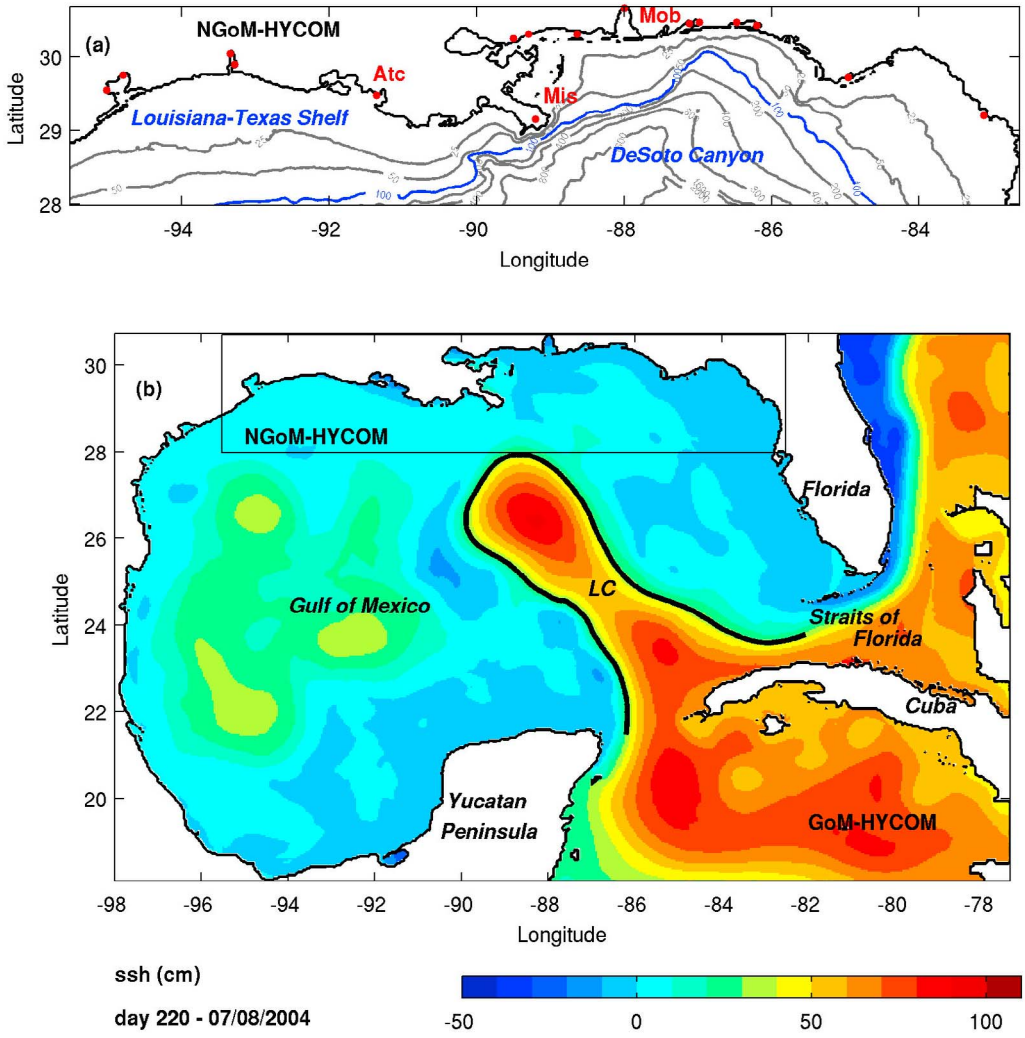

Figure 1. (a) NGoM-HYCOM model. Selected isobaths are shown and the shelf break (100 m isobath) is highlighted in blue. The location of major rivers where freshwater discharges are imposed are shown as red dots (Atc, Atchafalaya; Mis, Mississippi; Mob, Mobile Bay). (b) SSH (in cm) from the GoM-HYCOM model on 7 August 2004. The location of the NGoM-HYCOM model is shown. The thick black line represents the LC SSH 17 cm contour that is employed to track the maximum latitude of the LC in time (section 4).

Li et al., 1997; *Nowlin et al.*, 2005], and the local wind is a major controlling factor over the surface circulation, structure and transport pathways of the MR plume [*Walker*, 1996; *Walker et al.*, 2005a]. Easterly winds (southeasterly to northeasterly, prevalent during autumn, winter and spring) drive westward surface currents along the south side of the delta, extend the MR plume toward the Louisiana-Texas shelf and promote accumulation of low-salinity waters, sediments and nutrients on the shelf between the Mississippi and Atchafalaya deltas. This pattern is frequently disrupted by short-term wind reversals that occur due to the passage of colds fronts, which can reverse the direction of the coastal current, plume transport, and promote eastward and offshore dispersal of plume waters [*Walker et al.*, 2005a]. In the summer, the seasonal shift to more southerly winds also reverses the plume circulation and promotes an eastward transport of riverine waters toward the DeSoto Canyon [*Walker et al.*, 1994; *Morey et al.*, 2003a].

[4] The offshore circulation in the GoM is dominated by the energetic Loop Current (LC, Figure 1b) and mesoscale eddies. The LC is characterized by a cycle of northward penetration and westward bending until it reaches an unstable configuration, which leads to the shedding of an anticyclonic eddy (Loop Current Eddies, LCEs) [*Maul*, 1977; *Vukovich et al.*, 1979; *Hurlburt and Thompson*, 1980; *Huh et al.*, 1981]. This shedding process happens at intervals from 3 to 17 months [*Sturges and Leben*, 2000] and after LCEs are shed, they drift into the western GoM where they decay against the continental margin. Cyclonic frontal eddies (Loop Current Frontal Eddies, LCFEs) propagating clockwise along the LC front are also part of the system [*Paluszkiewicz et al.*, 1983; *Vukovich*, 1986; *Fratantoni et al.*, 1998; *Walker et al.*, 2003; *Chérubin et al.*, 2006]. The interaction of the LC system with shelf waters in the NGoM has been documented previously [*Huh et al.*, 1981; *Schroeder et al.*, 1987; *Walker et al.*, 1994; *Muller-Karger*, 2000; *Nowlin et al.*,

2000; *Hamilton and Lee*, 2005], and pronounced eddy energy and cross-shelf flows have been observed in the vicinity of the MR outflow [*Ohlmann et al.*, 2001]. In this region, filaments of low-salinity waters can be entrained by the LC or LCEs when they impinge against the shelf break [*Morey et al.*, 2003b; *Walker et al.*, 2005a]. This facilitates the likelihood for MR waters to be transported along the edge of the LC down to the Straits of Florida [*Walker et al.*, 1994; *Ortner et al.*, 1995; *Gilbert et al.*, 1996; *Hu et al.*, 2005]. Direct offshore removal of MR waters induced by storms and strong wind events, followed by subsequent entrainment by slope eddies, has also been reported [*Walker et al.*, 1996, 2005b; *Yuan et al.*, 2004; *Stone et al.*, 2005].

[5] The above circulation patterns make the MR plume a unique study case of the development of a large river plume in the presence of a complex scenario, where variable wind forcing, complex bottom and coastal topography, along with interactions with a strong boundary current and a rich eddy field, are integral parts of the plume dynamics. The overarching objective of this study is to expand river plume studies (that generally are confined on the coastal and shelf areas) to the interaction with shelf break and offshore flows. Specific objectives are the development and evolution of the MR plume under realistic circulation forcing mechanisms on the northern gulf shelf and on the gulf interior, and the synergy of these mechanisms with the complex topography near the MR delta on the offshore exportation of riverine waters.

[6] By elucidating the cross-marginal transport due to both shelf and offshore currents, new insights can be gained on the connectivity of the MR wetlands and remote coastal systems. Our methodology concentrates on the development of a high-resolution (1/50°, ~1.8 km) regional hydrodynamic model of the NGoM region and on a realistically forced numerical simulation that employs high-frequency atmospheric forcing and lateral boundary conditions. The NGoM domain is nested within a lower-resolution (1/25°, ~3.6 km), data-assimilative regional GoM model which provides realistic lateral boundary conditions that incorporate the LC and mesoscale eddy circulation. The fate of MR waters is evaluated in terms of estimates of freshwater transport, and events that demonstrate the impact of the offshore circulation on the plume dynamics are investigated and compared to observations. This paper is organized as following: A description of the numerical model developed for this study is provided in section 2, and the experiment setup is described in section 3. Results are presented in section 4, followed by a discussion in section 5. Conclusions are presented in section 6.

2. Model Description

2.1. The HYCOM Model

[7] The Hybrid Coordinate Ocean Model (HYCOM; http://hycom.org) is employed in this study to investigate the dynamics of the MR plume. HYCOM is a primitive equation ocean general circulation model supported by code development and operational global/regional simulations associated with the HYCOM consortium for Data Assimilative Modeling. HYCOM is designed as a finite difference, hydrostatic, Boussinesq model intended to use isopycnal vertical coordinates throughout as much of the stratified ocean interior as possible, while performing a dynamical transition to fixed vertical coordinates (either terrain following or z levels) in regions where isopycnal coordinates are suboptimum, such as the surface mixed layer or unstratified seas [*Halliwell et al.*, 2009]. Although initially applied on the study of large-scale, open ocean processes, the philosophy behind the transformable vertical coordinate system is particularly attractive when addressing coastal to offshore interactions.

[8] Detailed description of the model fundamental properties, such as governing equations and numerical algorithms, is presented by *Bleck* [2002], *Chassignet et al.* [2003] and *Halliwell* [2004] and in the model manual at http://hycom.org. HYCOM contains different choices of vertical mixing schemes [*Halliwell*, 2004], and in this study we employ the K profile parameterization model (KPP) [*Large et al.*, 1994] with a modification that includes an explicit parameterization of the bottom boundary layer [*Halliwell et al.*, 2009]. The KPP scheme was successfully employed by *Halliwell et al.* [2009] and *Kourafalou et al.* [2009] in coastal simulations with strong wind and buoyancy forcing. *Schiller and Kourafalou* [2010] employed KPP in experiments to study the dynamics of large-scale river plumes, and it was shown that the use of a different mixing scheme did not impact the plume vertical structure. *Schiller and Kourafalou* [2010] also developed an updated parameterization of the river inflow in HYCOM. We apply the parameterization presented therein in the Mississippi River inflow and other freshwater sources in the NGoM-HYCOM model (Figure 1a).

2.2. The NGoM-HYCOM Model

[9] The NGoM-HYCOM model is an application of HYCOM as a high-resolution domain (Mercator mesh of 1/50°, about 1.8 km) that covers part of the northern Gulf of Mexico. It was developed for this study and includes the majority of the northern gulf coastline, extending from the Big Bend region in the Florida Panhandle to part of the northern Texas coastline (Figure 1a). Bottom topography is derived from the 2 min NAVO/NRL DBDB2 global data set with true coastline, minimum depth of 2 m and maximum depth of about 3000 m in the interior of the DeSoto Canyon. Thirty hybrid vertical levels are employed. In the upper 40 m of the water column, we impose 15 permanent fixed levels (i.e., levels that cannot revert to isopycnal layers) which transit from z levels that are spaced 0.25 m apart close to the coastline, to terrain-following (sigma) levels over the inner continental shelf and back to z levels in midshelf waters. The transition of the sigma levels back to z levels occurs when the thickness of each vertical level reaches a predetermined maximum value that ranges from approximately 1 to 5 m (increasing downward). This feature gives the model layers the flexibility to have a variable distribution throughout the domain. Model layers quickly transform from sigma to z levels in regions of steep topography (east of the MR delta) and remain as sigma levels for a longer extent over regions where the continental shelf is wider (west of the MR delta). An example of the distribution of vertical levels is illustrated in Figure 2e. Below 40 m of depth, vertical levels are initialized as isopycnal layers (thicknesses increasing from approximately 20 to 500 m toward the bottom) and may transform to z levels, if necessary. This

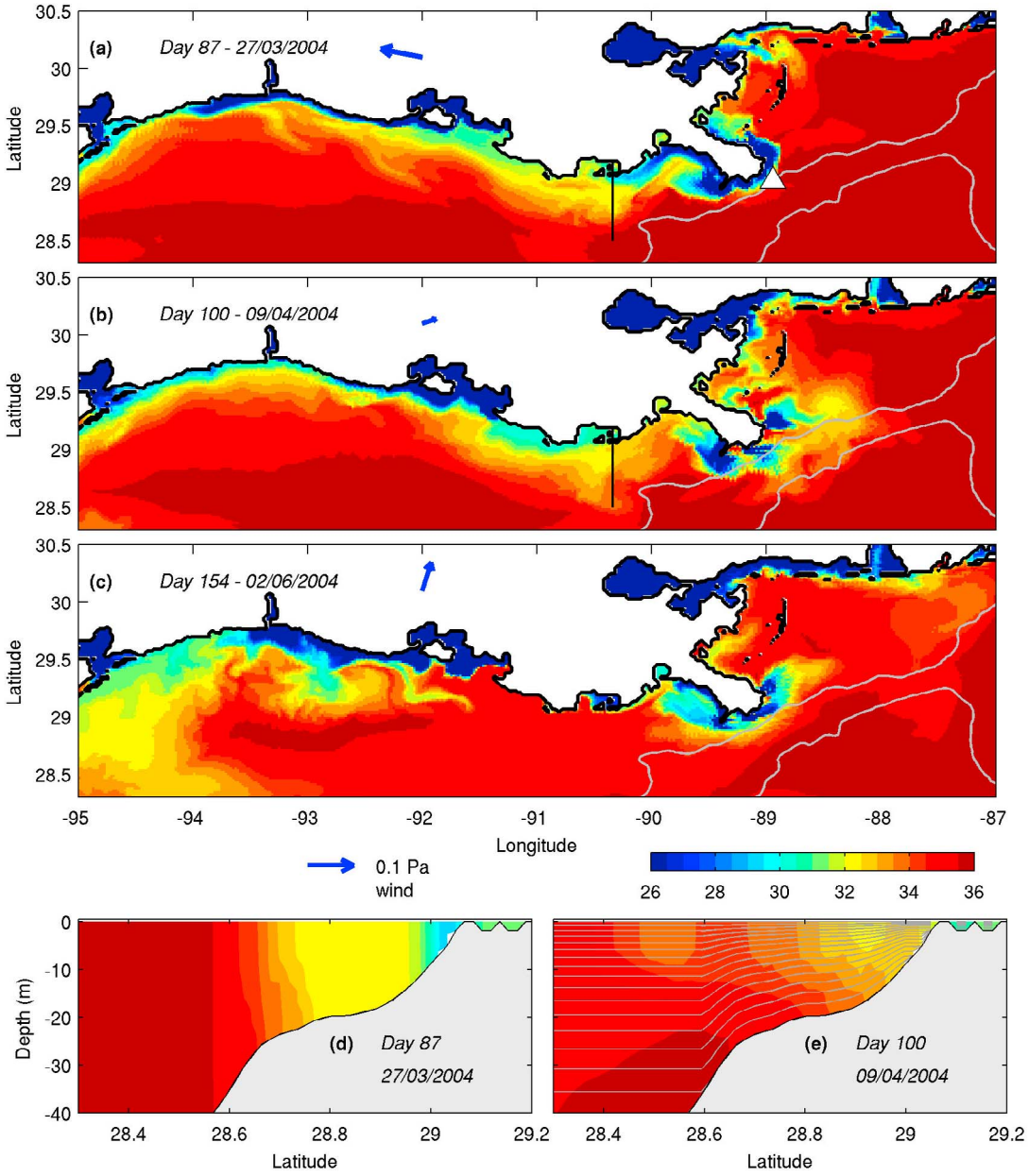

Figure 2. Sea surface salinity from selected days depicting different conditions of the MR plume (part of the model domain shown): (a) during a period of easterly, downwelling-favorable winds; (b) after a period of westerly, upwelling-favorable winds and (c) during a period of southerly winds. The gray lines represent the 100 and 1000 m isobaths. The blue vector shows the average wind direction during each event at a point in front of the MR delta (white triangle). The black line shows the location of the vertical sections of salinity presented for (d) day 87, easterly winds and (e) day 100, westerly winds. Salinity values less than 26 are not shown. The vertical layers in the upper water column at the location of the section are illustrated in Figure 2e as gray solid lines.

particular distribution of vertical levels is chosen such that adequate vertical resolution in the upper water column always exists to resolve the vertical structure of the MR plume. *Schiller and Kourafalou* [2010] suggest that when simulating river plumes, permanent fixed levels (either sigma or z) should be imposed in the upper water column. The reason is to prevent isopycnal layers from interacting with the bottom of the buoyant plume, which could be detrimental for the vertical structure of the plume. The reader is referred to *Schiller and Kourafalou* [2010, Figure 13] for further illustration of this structure of vertical coordinates. The current choice to have half of the vertical levels as isopycnal layers is based on the fact that this study also involves the simulation of mesoscale eddies and deep ocean currents generated by LC features, and isopycnal layers provide optimal resolution for such oceanic processes.

[10] Lateral open boundaries are on the southern boundary and part of the western boundary of the domain. At the coastal wall, the normal velocity is zero and a no-slip condition is used for the tangential velocity. There is no flow normal to the topography. At the bottom, momentum is dissipated by a quadratic bottom drag (drag coefficient $C_d = 3 \times 10^{-3}$), using a bottom velocity u_b that represents the average velocity in a slice of water situated just above the bottom. The thickness of this slice is determined by the bottom boundary layer parameterization from the KPP scheme [*Halliwell et al.*, 2009]. Salt and heat fluxes normal to the bottom and to the coast are set to zero.

[11] Freshwater sources (Mississippi River plus other sources, Figure 1a) are prescribed following the updated parameterization by *Schiller and Kourafalou* [2010], which includes the introduction of a mass inflow parameterization, and choices to specify the downward penetration and the lateral spreading of the river inflow. Point-source discharges were included for all northern gulf rivers, except for the Mississippi River, where the discharge was prescribed at the locations of the Southwest Pass, South Pass and Pass a Loutre. In order to reduce the low-salinity spike that may be created when all river discharge is concentrated in a few grid cells, we imposed a downward penetration of 4 m and a minimum spreading to surrounding grid points at all freshwater sources. The reproduction of smaller-scale, near-field outflow dynamics described by *Wright and Coleman* [1971] is beyond the scope of this study. We focus on the far-field properties of the MR plume.

3. Numerical Simulation

[12] The realistically forced experiment covers a period of 2 years, from 1 January 2004 to 31 December 2005. High-frequency (3 hourly) atmospheric forcing is derived from a regional coupled ocean-atmosphere simulation performed with the Coupled Ocean/Atmospheric Mesoscale Prediction System (COAMPS) [*Hodur et al.*, 2002] with a horizontal resolution of 27 km. The surface boundary is forced by fields of wind stress, air temperature, radiation exchanges (incident solar radiation + radiation emitted by the surface) and precipitation. Surface latent heat (evaporation) and sensible heat fluxes are calculated using the parameterization scheme of *Kara et al.* [2005]. Daily averaged freshwater discharges are prescribed for all sources marked in Figure 1a (except for Mobile Bay and Pearl River where monthly climatologies are imposed). A twin experiment without river forcing also took place to allow the calculation of freshwater fraction (section 4.1).

[13] In order to apply open boundary conditions that realistically introduce the circulation induced by the LC, LCE and other mesoscale eddies, the NGoM-HYCOM model is nested within the regional GoM-HYCOM model which has horizontal resolution of 1/25° and 20 hybrid layers in the vertical (Figure 1b) [*Prasad and Hogan*, 2007; *Kourafalou et al.*, 2009; *Halliwell et al.*, 2009]. The GoM-HYCOM simulation used herein employs the Navy Coupled Data Assimilation system (NCODA) [*Cummings*, 2005], which is an oceanographic version of the multivariate optimum interpolation technique commonly employed in atmospheric forecasting systems. The NCODA system assimilates satellite altimetry track-by-track and sea surface temperate (SST) directly from orbital data using model forecasts as the first guess. Although the system assimilates more data types, the limited availability of in situ observations in the open GoM makes the assimilation scheme to rely primarily on satellite altimetry and SST measurements. *Kourafalou et al.* [2009] showed the realistic representation of the LC variability in the NCODA based GoM-HYCOM simulation, as compared to a free running, twin simulation. Nesting to the NGoM-HYCOM domain is done in off-line mode (archived files). A dynamical boundary condition is applied for which no distinction is made between the inflow and outflow boundaries [*Halliwell et al.*, 2009]. The method of characteristics is used to solve the barotropic flow fields (velocity and pressure) [*Browning and Kreiss*, 1982, 1986] and a nesting relaxation zone (10 grid points wide with e folding time of 0.1–24 days) is used to relax the baroclinic structure (temperature, salinity, pressure and velocity) toward the fields provided by the GoM-HYCOM model.

4. Results

[14] Although the Mississippi River is the primary source of low-salinity waters in the northern gulf, the contribution of several other freshwater sources results in a low-salinity band along the northern coast. The dynamics of the broad MR plume and the low-salinity coastal band in the vicinity of the MR delta are highly affected by the wind conditions and the bottom and coastal topography. Figure 2 presents examples of different states of the MR plume and low-salinity band under distinct wind conditions. During a period of easterly winds (Figure 2a), plume waters are transported to the west of the MR delta, following the westward downwind coastal current. Because the main orientation of the coast line is in the east-west direction, the dynamics correspond to the response of a buoyant plume to downwelling-favorable winds [*Csanady*, 1978; *Chao*, 1988; *Kourafalou et al.*, 1996a]. Easterly winds promote an onshore Ekman transport and a downwind drift at the coast, while the low-salinity band is confined against the coast. The vertical structure of the plume in the coastal current region (Figure 2d) demonstrates that the downwelling-favorable winds can efficiently mix the plume in the vertical. The offshore extent of the plume is reduced in the vicinity of the delta, since plume waters are transported onshore and westward. The transport of low-salinity waters toward the broader Louisiana-Texas shelf effectively insulates the coastal plume from the offshore circulation beyond the shelfbreak (100 m isobath). As a consequence, interactions of the MR plume with shelfbreak and offshore eddies is unlikely to happen during easterly wind events.

[15] The offshore transport of plume waters is enhanced in the presence of westerly, upwelling-favorable winds (Figure 2b). To the west of the delta, the eastward downwind drift at the coast reverses the buoyant coastal current, and low-salinity waters are transported offshore due to surface Ekman dynamics (Figure 2e) [*Chao*, 1988; *Fong and Geyer*, 2001]. The result is a broadening of the low-salinity coastal band. The proximity of the shelf break to the MR delta maximizes the offshore transport of plume waters in that region. Low-salinity riverine waters are transported eastward and offshore, toward the rim of the DeSoto Canyon, a process that facilitates the interactions between the

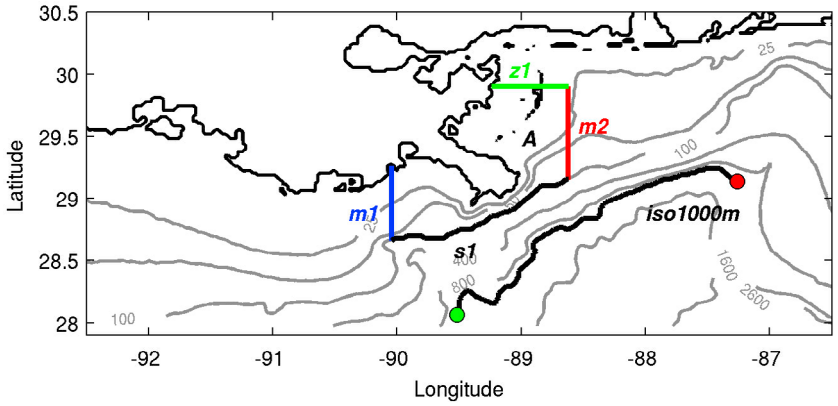

Figure 3. Location of the sections (m1, m2, z1, s1 and iso1000m) where freshwater transport analysis is performed. The area *A* represents the region where wind stresses are spatially averaged. Selected isobaths are shown (solid gray lines). The dots on section iso1000m show the initial (green dot) and final (red dot) points of the along-section distance in Figures 7 and 8.

plume and the offshore circulation. Offshore transport of low-salinity waters is also induced in the presence of southerly southwesterly winds (Figure 2c). Although the onshore winds cause retention of MR plume waters on the west side of the delta, low-salinity waters are also transported eastward and along the shelf break. This process is attributed to the surface Ekman transport that develops in the vicinity of the delta [*Morey et al.*, 2003a]. The response of the plume is different on the Louisiana-Texas shelf. Due to the variations in the local coastal topography, the onshore winds promote a divergence of waters within the low-salinity band between the Atchafalaya and the MR deltas. This disrupts the coastal current and erases the plume signal along the Louisiana-Texas shelf.

4.1. Shelf Transport of Plume Waters Around the MR Delta

[16] The pathways and the overall fate of MR plume waters are first investigated by computing the freshwater transport Q_{fw} across four sections that establish a closed region around the MR delta (m1, m2, z1 and s1, Figure 3). Q_{fw} was computed as

$$Q_{fw} = \int\int_{-h}^{\eta} fw_f V dz dx,$$

where V is the horizontal velocity normal to the section, η is the sea level, h is the bottom depth and the integral with respect to x is the horizontal distance along the section. The freshwater fraction fw_f is equal to $fw_f = \frac{S_b - S}{S_b}$, where S_b is the background undiluted salinity and S is the diluted salinity due to the river discharge. S_b was obtained from a twin experiment that was forced by the same atmospheric and lateral boundary fields but without river inflows. Q_{fw} was further separated into barotropic and baroclinic components, and the total Q_{fw} is given by

$$\begin{aligned} Q_{fw}total &= Q_{fw}barotropic + Q_{fw}baroclinic \\ &= \int\int_{-h}^{\eta} fw_f V_{btrop} dz dx + \int\int_{-h}^{\eta} fw_f V_{bclin} dz dx, \end{aligned}$$

where V_{btrop} and V_{bclin} are the barotropic and baroclinic components of the across-section velocity, respectively.

[17] First, we estimated the relative importance of the barotropic and baroclinic currents for the flow structure and Q_{fw} at sections m1, m2, z1 and s1. This estimate was based on the ratio of the mean baroclinic Eddy Kinetic Energy (EKE) to the total EKE (see *Teague et al.* [2006] for details). R_{eke} is defined as

$$R_{eke}(z) = \frac{\overline{u_{dd}'^2(z)} + \overline{v_{dd}'^2(z)}}{\overline{u'^2}(z) + \overline{v'^2}(z)},$$

where $\overline{u'^2}(z)$ and $\overline{v'^2}(z)$ are the total velocity variances and $\overline{u_{dd}'^2}(z)$ and $\overline{v_{dd}'^2}(z)$ are the variances of the baroclinic component of the velocity. Daily outputs of model velocities from the two years of simulation were used in this analysis. R_{eke} provides the fraction of the total velocity variance that is explained by baroclinic currents. If $R_{eke} = 0$, currents are mostly barotropic. If $R_{eke} \geq 1$, currents are mostly baroclinic.

[18] Figure 4 shows the vertical structure of R_{eke} along the four sections. At section m1 (Figure 4a), the R_{eke} has low values (<0.3) in the interior of the water column, indicating that barotropic processes account for more than 70% of the EKE in middepth layers. Values slightly higher (~0.5) are observed at the surface, which are associated with buoyancy effects induced by the river discharge. Close to the bottom, R_{eke} was equal to or larger than 1, suggesting strong velocity shears associated with a bottom Ekman layer and cross-shelf flows. The structure of R_{eke} at sections m2 and z1 (Figures 4b and 4c) is similar to the one from section m1, although a larger portion of the water column has values lower than 0.3. In contrast to the other sections, section s1 (Figure 4d) presents a more defined surface layer (10–15 m deep) where R_{eke} was close to 0.6 and baroclinic processes contributed more to the EKE. In spite of the large layer in the interior of the water column where EKE is mostly barotropic, a large bottom layer with $R_{eke} > 1$ exists and that represents the effect of strong velocity shears and bottom intrusions from the offshore region.

[19] The R_{eke} analysis suggests that Q_{fw} is largely barotropic across sections m1, m2 and z1, whereas Q_{fw} could present a

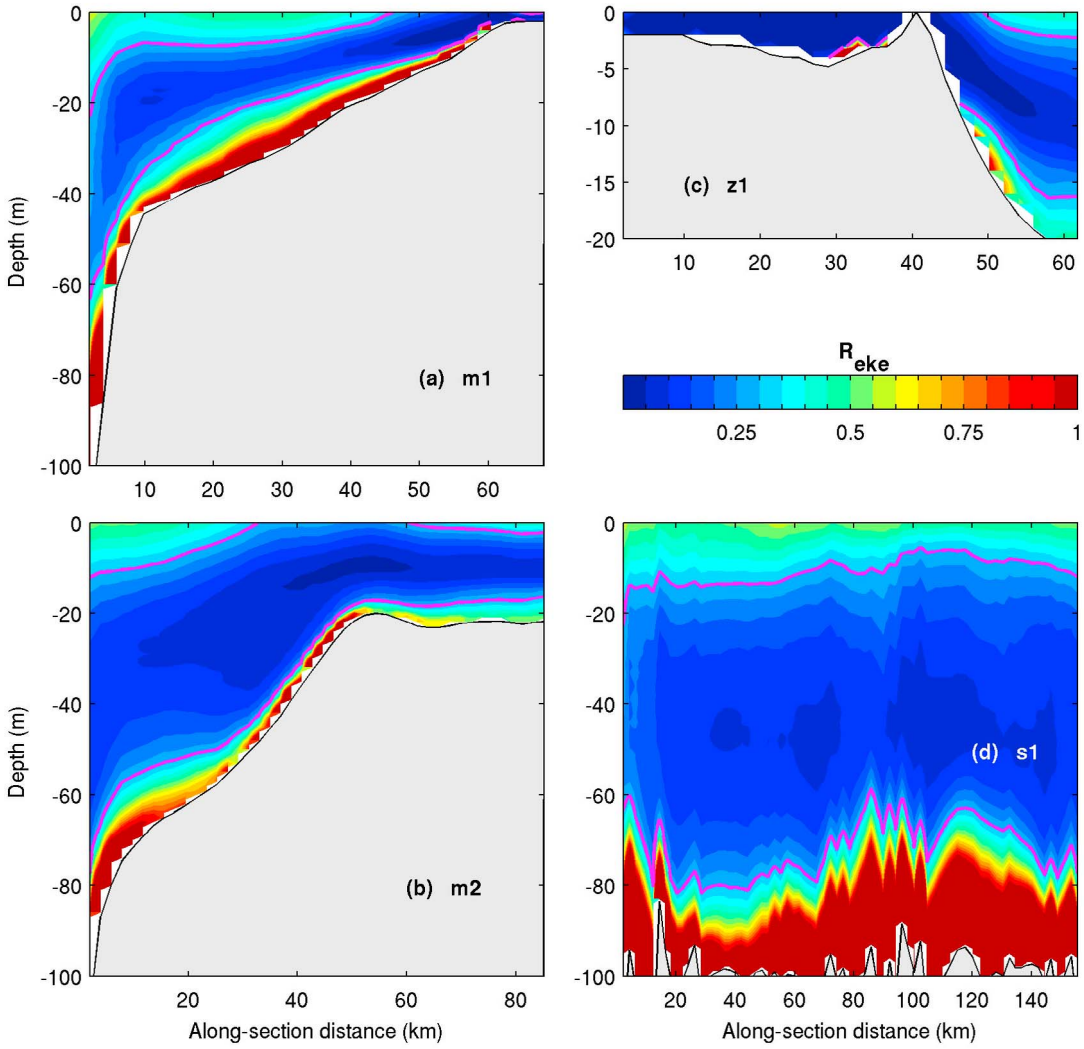

Figure 4. Vertical structure of the kinetic energy ratio R_{eke} at sections m1, m2, z1 and s1 (marked in Figure 3). The magenta line represents the 0.3 contour. Values above 1 are not shown.

stronger baroclinic signal across section s1. Figure 5 presents estimates of barotropic Q_{fw} and baroclinic Q_{fw} across sections m1, m2, z1 and s1 for the two years of simulation, together with time series of wind stress components that were spatially averaged over area A (Figure 3). Wind events that favor the transport of plume waters toward the offshore region, and therefore the interaction with the offshore eddy circulation, are identified as W1–6. Those wind events constitute periods of winds with a strong westerly component or periods of southerly/southwesterly winds. In agreement with the R_{eke} analysis, Q_{fw} across m1 (Figure 5b) and across m2 (Figure 5c) is mostly barotropic. The barotropic Q_{fw} across both sections is well correlated with the across-section wind stress (east-west); the linear correlation coefficient r is equal to 0.68 at m1 and equal to 0.45 at m2. The larger correlation at m1 is attributed to the proximity of m1 to the coast line, where the flow is constrained by the coastal topography. At m2, the open shelf introduces a larger variability in the direction of the flow.

[20] The largest wind-driven, eastward transports of plume waters across m2 and toward the DeSoto Canyon were observed during W2 and W5, which are periods in the spring and spring-summer transition when the winds developed a southerly/southwesterly direction. W2 and W5 were prolonged periods that lasted for approximately 2 months each. With the exception of a few reversals, the freshwater transport was mostly eastward with the total Q_{fw} (barotropic plus baroclinic) peaking at 1.6 (W2) and 2.8 (W5) $\times 10^4$ m^3s^{-1}. Shorter wind events with easterly or southerly components are also observed in the spring (W1) and the summer (W6), and they also contribute to eastward transports that were short in duration with peaks ranging from 0.5 to 1.2 $\times 10^4$ m^3s^{-1}. In the autumn (W3) and winter (W4), eastward transport of plume waters is observed in the presence of brief periods of strong westerly winds and the passage of cold fronts.

[21] The freshwater transport across z1 is basically barotropic (Figure 5d) and is well correlated with the north-south wind stress (linear correlation of 0.63). The lower magnitude of the barotropic Q_{fw} demonstrates that a small fraction of MR waters is transported northward. The largest northward transport across z1 also corresponds to an event of

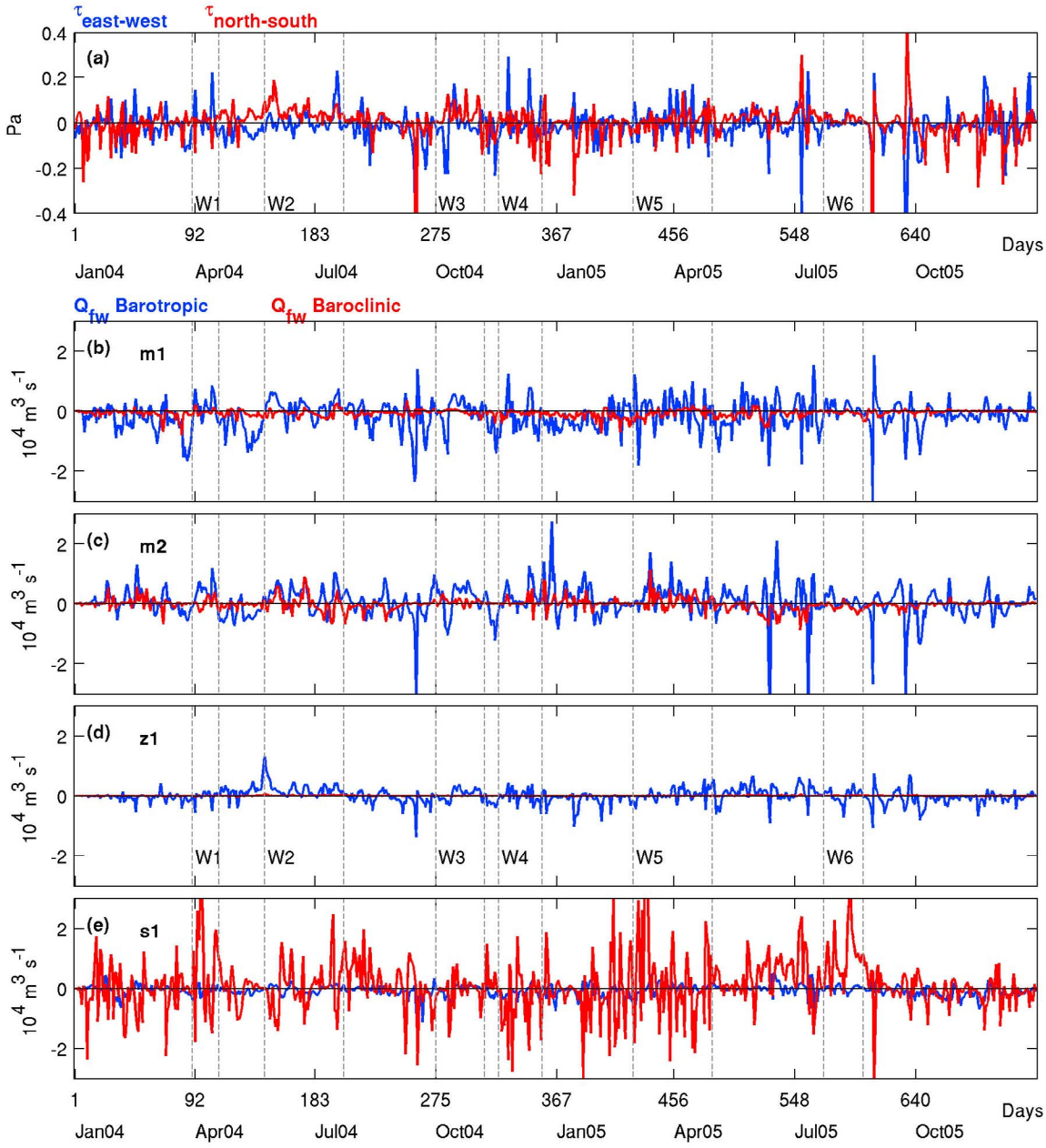

Figure 5. (a) Time series of wind stress components computed as spatial averages from area *A*. Selected wind periods for further analysis are delimited by vertical dashed gray lines and are identified as W1–6. Time series of barotropic and baroclinic freshwater transport Q_{fw} across sections (b) m1, (c) m2, (d) z1 and (e) s1 (marked in Figure 3). Positive/negative values represent eastward/westward transport across sections m1 and m2, northward/southward transport across section z1 and onshore/offshore transport across section s1.

southerly winds at the beginning of period W2 (Q_{fw} total = 1.3×10^4 $m^3 s^{-1}$). Southward pathways mostly correspond to the transport of freshwater from sources in the Mississippi-Alabama coast and toward the MR delta. Finally, Q_{fw} across s1 has different characteristics than across the other sections (Figure 5e), since the magnitude of the baroclinic transport is much larger than the magnitude of the barotropic transport. That corroborates with the R_{eke} structure from section s1, which presents a surface layer where the baroclinic currents are more than or as equally energetic as the barotropic currents. The baroclinic Q_{fw} across s1 presents larger variability and magnitude than across the other shelf sections, and the correlation with the wind is less clear. That is attributed to the fact that s1 is located at the shelf break and is very close to the freshwater source; fast changes in the wind direction could disperse large volumes of plume waters on and off the shelf. In the absence of winds, plume waters could also expand offshore. Low-salinity waters are advected away from the delta and toward the shelf break (negative baroclinic Q_{fw}) more frequently during the winter

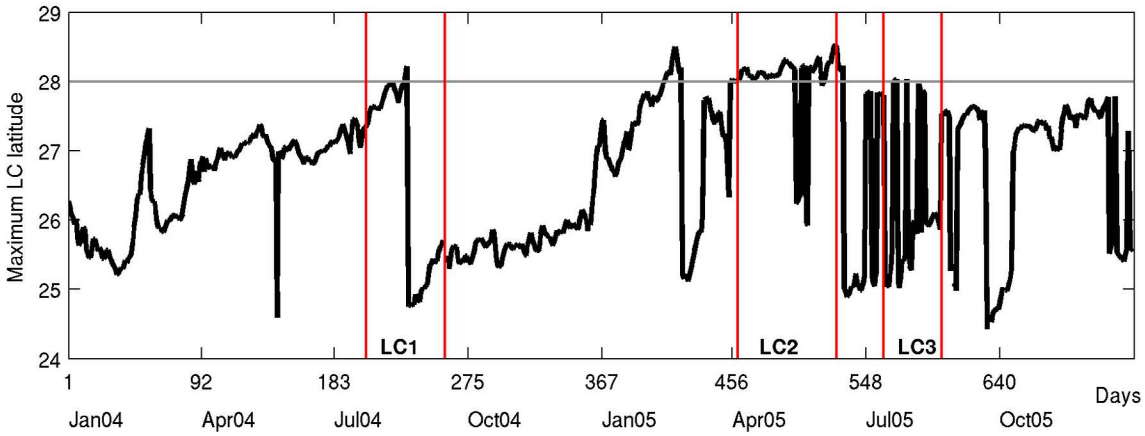

Figure 6. Time series of the maximum latitude of the LC calculated from the full GoM-HYCOM regional model. The maximum latitude is based on the northernmost point of the LC SSH 17 cm contour exemplified in Figure 1b. Three periods of LC impact on the MR dynamics that are further investigated are shown (LC1, 2 and 3) and are delimited by vertical red lines. The horizontal gray line represents the latitude of the southern open boundary of the nested NGoM-HYCOM model.

and spring months, when the offshore transport can reach -2×10^4 m^3 s^{-1}. In the end of the spring and during summer months, the offshore transport becomes less significant since the plume waters are pushed against the MR delta by the southerly winds. Plume waters are then transported to the east and toward the rim of the DeSoto Canyon, where the buoyant plume can interact with the offshore circulation and be removed offshore. The above results elucidate the processes controlling the interaction between wind and buoyancy-driven flows on the NGoM shelf. They are not intended as a study of seasonal variability, which requires a longer simulation.

4.2. Offshore Transport of MR Plume Waters

4.2.1. Loop Current Extension During 2004–2005

[22] The offshore removal of the MR plume into the interior of the GoM is directly related to the proximity of the LC system and mesoscale eddies to the shelf break, where they may entrain riverine waters. The interactions between the MR plume and the LC system should take place when the LC is well extended and close to the shelf break of the NGoM region, or when an LCE is shed and it intrudes into the NGoM. In order to identify the periods of time when MR plume dynamics may be affected by the LC system, we tracked the LC northernmost position in time using a technique presented by *Leben* [2005]. Daily sea surface height (SSH) fields from the GoM-HYCOM simulation that provided boundary conditions to the NGoM-HYCOM model were used to determine the boundary of the LC and its maximum latitude. The boundary of the LC is defined as the 17 cm SSH contour that extends from the Yucatan Channel to the Straits of Florida, and it is exemplified as a black solid line in Figure 1b. The 17 cm SSH contour is selected as a proxy for the high-velocity core of the LC, and this parameter was previously used to track the LC evolution and shedding of LCEs with success by *Leben* [2005]. On each day, we identify the maximum latitude of the 17 cm SSH contour to determine the northward penetration of the LC.

[23] The time series of the LC maximum latitude (Figure 6) shows the progressive evolution of the northward penetration of the LC. In spite of short-term variations, the northward penetration increases with time until it reaches a peak and drops abruptly when an LCE is shed. Events of LCE separation and reattachment are also observed as short, large negative oscillations in the maximum latitude time series. Three periods of LC impact and interaction with the MR plume are separated by vertical solid red lines and identified as LC1–3. During year 2004, the LC presented a very clear cycle of continuous northward penetration, shedding of an LCE in mid August and return to the port-to-port configuration (Yucatan to Straits of Florida). At the time of the eddy separation, the LC was well extended northward and the LCE intruded in the southern boundary of the NGoM-HYCOM model, therefore impacting the offshore circulation of the NGoM region (LC1 event). The LC does not present a clear cycle during year 2005, when a series of detachment and reattachment events took place. The LC system was well penetrated northward for several months, especially between the months of April and June when the LC was beyond 28°N and impacted the NGoM offshore circulation (LC2 event). That period is followed by a series of eddy detachment-reattachment events with the LC also intruding in the NGoM region (LC3 event). The variability observed in 2004–2005 is representative of the LC interannual variability [*Leben*, 2005].

4.2.2. Impact of Basin-Wide Circulation on the MR Plume

[24] The offshore transport of MR waters and the impact of the LC and other eddies are evaluated across a section located above the 1000 m isobath, which is just offshore of the shelf break in the vicinity of the MR delta (section iso1000m, Figure 3). Figures 7 and 8 present Hovmöller diagrams of SSH anomaly, across-section surface velocity and total Q_{fw} across the section iso1000m during years 2004 and 2005, respectively. On each day, the SSH anomaly represents the actual SSH along the section minus its average on that day. The SSH anomaly is useful to identify SSH variations

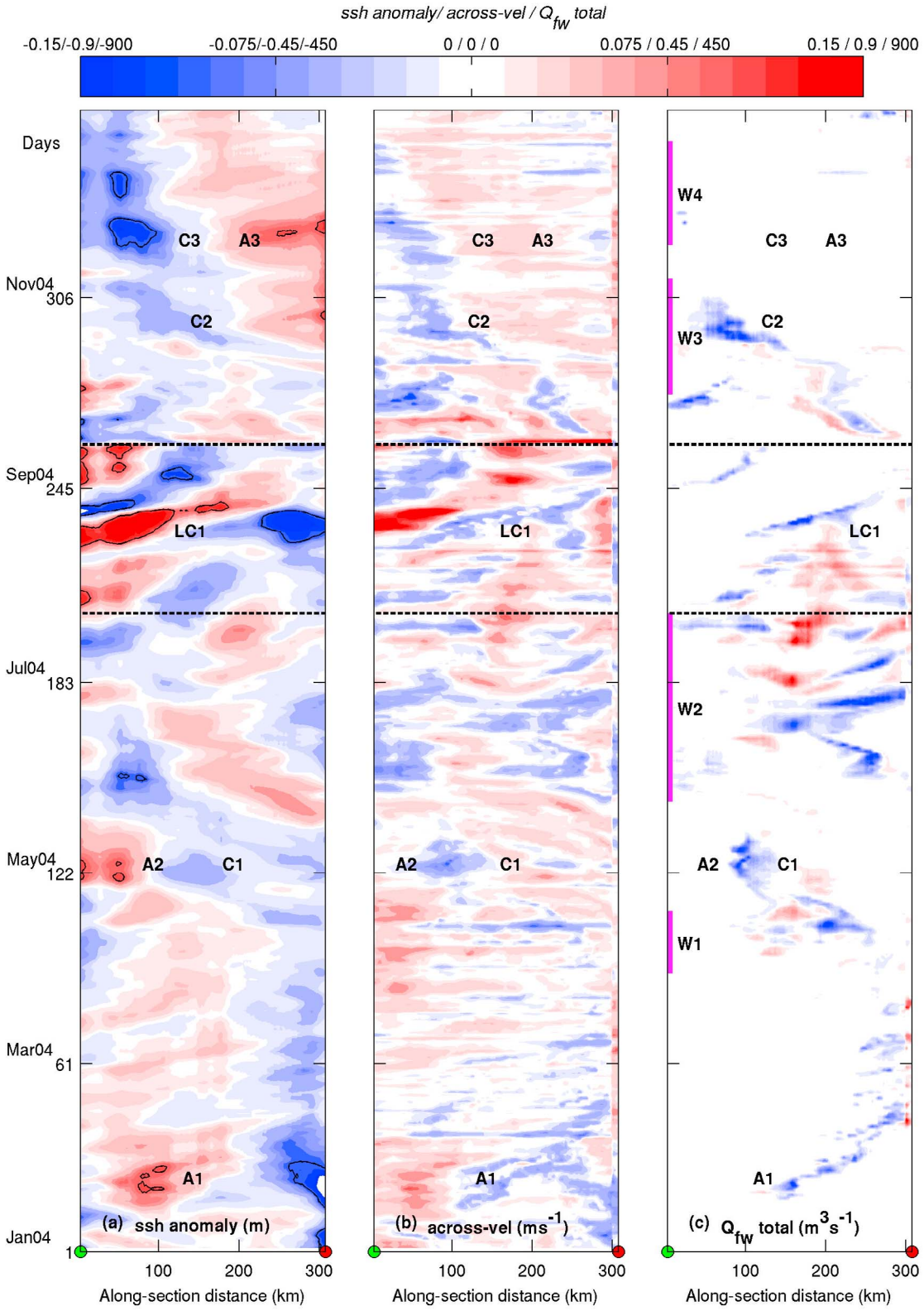

Figure 7. Hovmöller diagram of (a) SSH anomaly, (b) across-section surface velocity and (c) total freshwater transport Q_{fw} across section iso1000m for year 2004. Positive/negative values for onshore/offshore velocities and transports. The solid black line in Figure 7a represents the ±0.1 contour. Wind periods of interest are shown as vertical magenta lines in Figure 7c. Periods of LC impact are delimited by horizontal dashed black lines. Selected anticyclonic (A) and cyclonic (C) eddy events are shown. The orientation of the diagrams is given by the green and red dots and is shown in Figure 3.

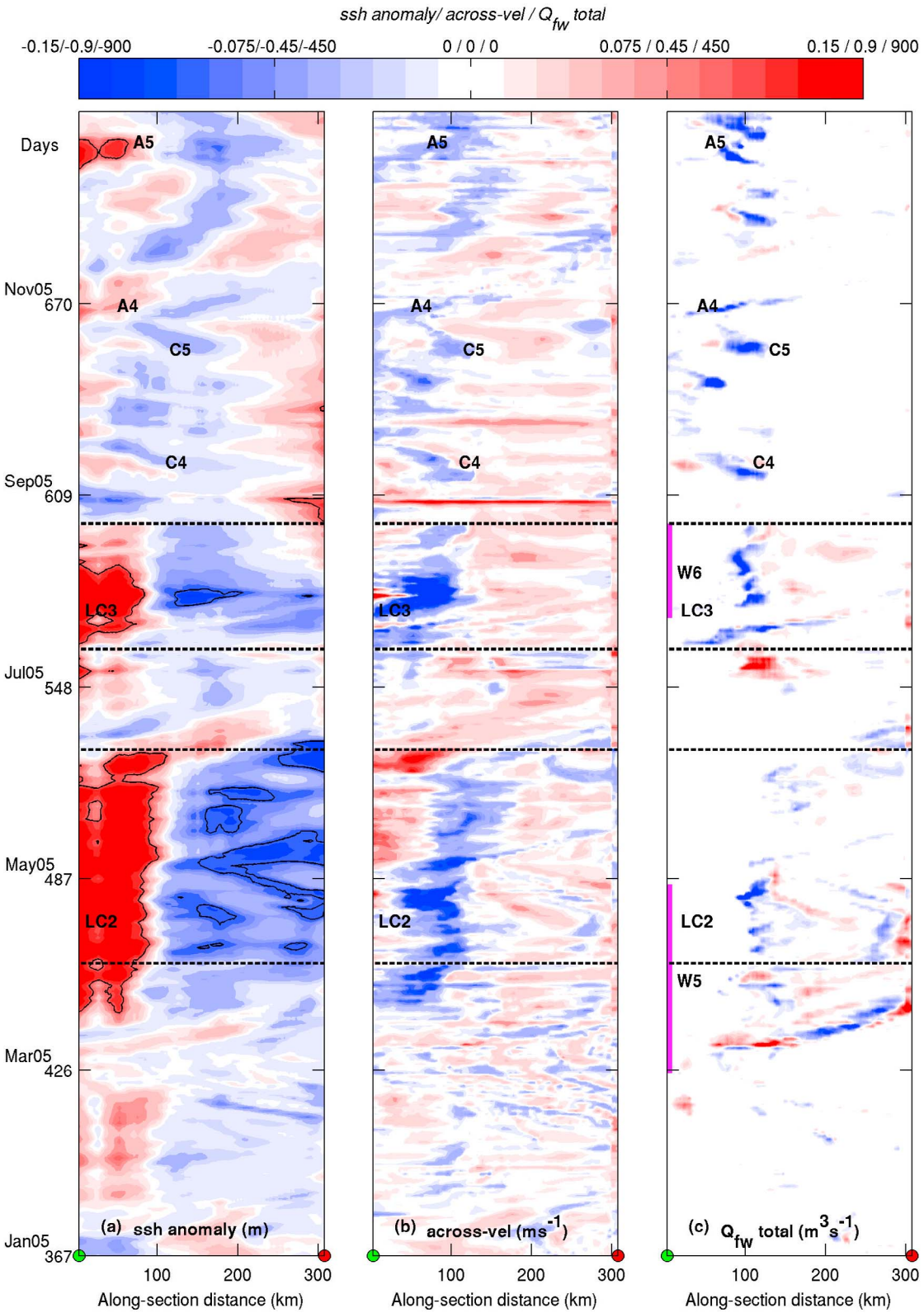

Figure 8. Same as Figure 7 but for year 2005.

associated with the passage of eddy structures. On year 2004 and during the event LC1, the passage of the tip of the LCE is observed as a strong, positive (anticyclonic) anomaly signal propagating eastward for several days in mid August (Figure 7a). This is immediately followed by a strong, negative (cyclonic) signal, which indicates the passage of a cold core eddy (LCFE). Throughout the year, several other eddy signals are observed to pass over the region, and major

events are labeled as A and C for anticyclonic and cyclonic eddies, respectively.

[25] At the time of the passage of the eddies, the response of the surface across-section velocity (Figure 7b) is coherent with the eddy circulation and the SSH anomaly distribution along the section. Onshore/offshore velocities are observed on western/eastern side of anticyclonic eddies, and vice versa for cyclonic eddies. As the eddy features propagate along the section, they induce offshore and onshore surface currents that determine the offshore removal of plume waters. Figure 7c shows the clear impact of the LCE and other eddies on the transport of the MR plume. During the LC1 period, streams of offshore (negative) Q_{fw} are observed as the eddy impinges against the shelf and propagates along the section. Other events of MR plume entrainment are also observed as other eddies (A1, A2, C1) travel through the region. The wind periods that promoted eastward transport of plume waters across m2 are also shown in Figure 7c (W1–4). With the exception of W4, riverine waters were removed offshore during all wind events, especially during W2 when very large volumes of freshwater were transported offshore in the presence of southerly/southwesterly winds. In spite of winds favoring offshore removal during W4, MR waters were not removed offshore due to the onshore circulation induced by eddies C2 and A3.

[26] Similar patterns of interactions between eddies and the MR plume are also observed during year 2005 (Figure 8). Large SSH anomalies are observed in the times when the LC intruded in the NGoM region (LC2–3, Figure 8a). For a period of approximately 2 months (LC2), the LC imposed persistent offshore surface currents across iso1000m (Figure 8b) and entrained freshwater from the shelf (Figure 8c). The entrainment of plume waters decreases substantially at the end of LC2 when a LCE is shed (Figure 6). The offshore transport only resumes when the LCE intermittently reattaches to the LC (event LC3). After that period, the LC system does not impact the NGoM region and other mesoscale eddies are responsible for the entrainment process (A4–5, C3–4).

4.2.3. Offshore Removal of MR Waters in the Presence of Southerly Winds (Events W2 and W5)

[27] Southerly/southwesterly winds during the period W2 lasted for approximately 2 months. In that time, large volumes of freshwater were transported eastward across m2 (Figure 5c), followed by offshore removal (Figure 7c). The LC system had not approached the NGoM region yet, and the entrainment of the plume was due to ambient circulation and eddies located in the DeSoto Canyon. Wind period W5 was also characterized by southerly/southwesterly winds, large eastward transport across m2 and subsequent offshore removal, although the LC system approached the NGoM region toward the end of the wind period (Figure 8c).

[28] The spatial structure of the plume and the interactions with the offshore circulation during those two events are exemplified in Figure 9. During period W2 (Figure 9a), the offshore circulation was characterized by a meandering westward flow (~0.5 m s^{-1}) and the presence of mesoscale eddies with 50–100 km in diameter. As the winds reverse the plume transport and advect the plume along the shelf break (days 154 and 157), the eddy circulation entrains the riverine waters and a coherent low-salinity band is formed along the offshore boundary current (day 160). The entrainment continues even after winds slightly push the plume onshore (day 163), and a few days later the offshore low-salinity band is dispersed by the offshore eddies (not shown). A similar scenario takes place during period W5 (Figure 9b), when the plume is advected toward the head of the DeSoto Canyon and is dispersed by the offshore circulation. Interestingly, the tip of the LC was located south of the MR delta (as seen by the anticyclonic circulation on days 443 and 446, ~0.8 m s^{-1}), but it did not take part in the offshore removal of the plume at that time. These results suggest that when the plume is captured by the mesoscale circulation it is unlikely to return to the shelf, even if the wind direction changes.

4.2.4. Entrainment of MR Waters by the LC System (Events LC1 and LC2)

[29] The interactions between the MR plume and the LC system are exemplified in Figure 10. Figure 10a demonstrates the intrusion of the LCE during the event LC1. The anticyclonic circulation of the LCE comes into close proximity to the MR delta, with currents reaching ~0.6 m s^{-1} at the shelf break region (day 233). As the tip of the eddy propagates eastward, it effectively entrains the MR plume and leads to the formation of a long and narrow low-salinity band that extends from the delta to the southern boundary of the domain (day 236). The presence of a cyclonic circulation over the shelf break enhances the process, and the dipole circulation induces offshore currents that reach 0.8 m s^{-1}. As the entrainment continues on the eastern side of the LCE, a cold core eddy advances on the western side of the LCE, and the onshore circulation shuts off the entrainment near the delta (days 239 and 242). A few days later (not shown), the tip of the LCE has moved to the east and the low-salinity band disappeared.

[30] The wind vectors in Figure 10a show that wind conditions were weak and unfavorable for the offshore transport, such that the removal of the plume was exclusively due to the proximity of the LC. The impact of the LC in the beginning of the period LC2 takes place in the presence of favorable winds (period W5, Figure 8c), but the LC continues to entrain riverine waters when winds become irregular and unfavorable for the offshore transport. At that time the LC is again close to the shelf break and efficiently entrains the MR plume, with the formation of a thin low-salinity tongue on the eastern side of the LC (Figure 10b, day 515).

4.3. Variability of MR Plume Offshore Pathways During 2004–2005

4.3.1. Freshwater Transport During Selected Events

[31] In order to better establish a relationship between the wind-driven, eastward transport of plume waters and the entrainment by the offshore circulation (LC and eddies), the negative values of total Q_{fw} from Figures 7c and 8c were integrated along the section iso1000m, collapsed into a single time series and plotted with the total Q_{fw} across m2 (Figure 11a). With the exception of W4, the eastward transport across m2 was followed by an offshore transport across iso1000m during all wind events. This behavior is particularly visible during the periods W2 and W5, when consecutive bursts of eastward transport were followed by peaks in the offshore transport of approximately same magnitude. Moreover, eddy events that overlapped favorable wind peri-

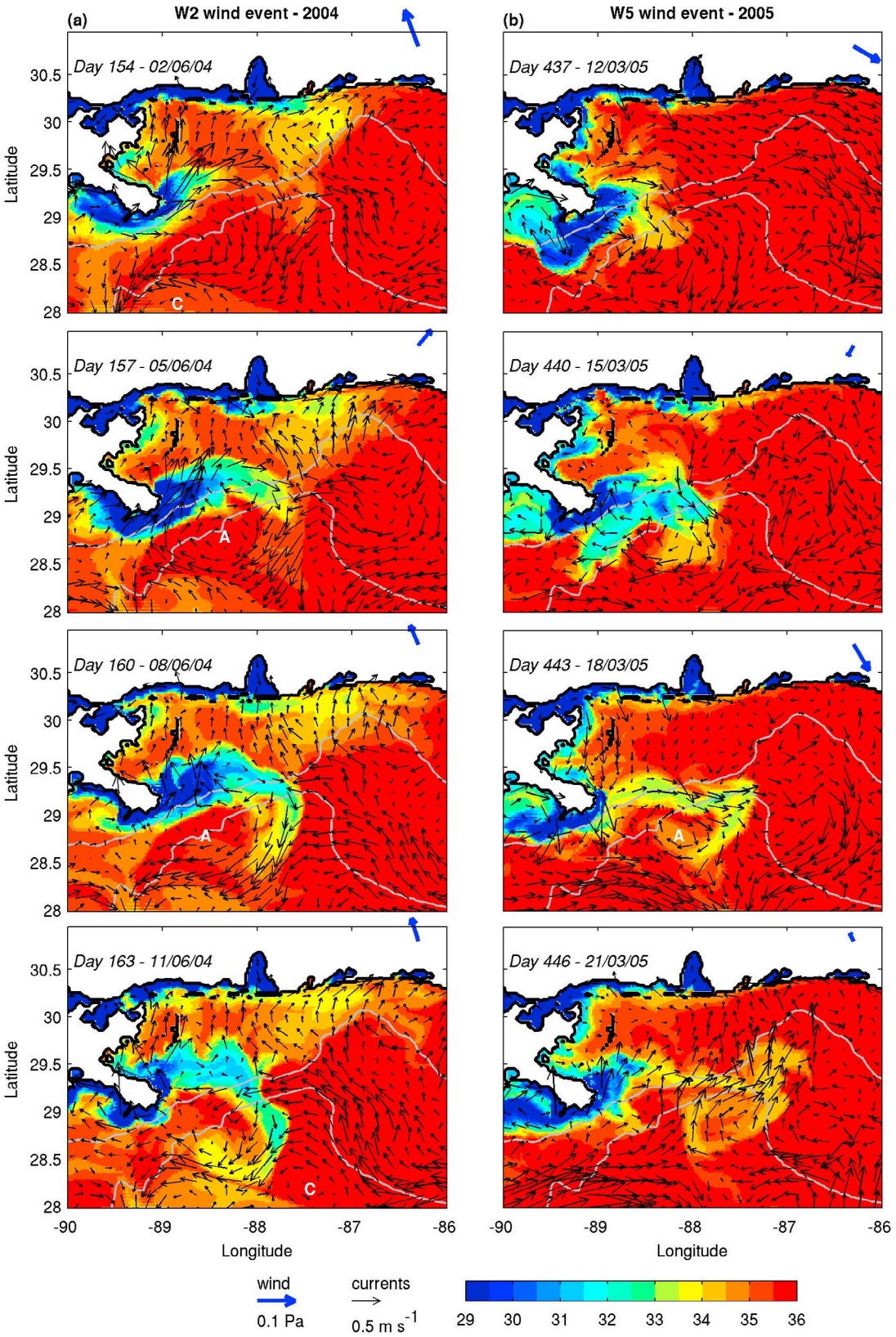

Figure 9. Snapshots of sea surface salinity and surface velocity vectors from selected days during the wind periods (a) W2 and (b) W5. Part of the model domain shown. Vectors are shown every other eight grid points for better visualization. The 100 and 1000 m isobaths are displayed as gray lines. A and C show the location of anticyclonic and cyclonic eddies, respectively. For each day, the wind stress vector averaged over the area *A* is presented on the upper right corner. Salinity values less than 29 are not shown.

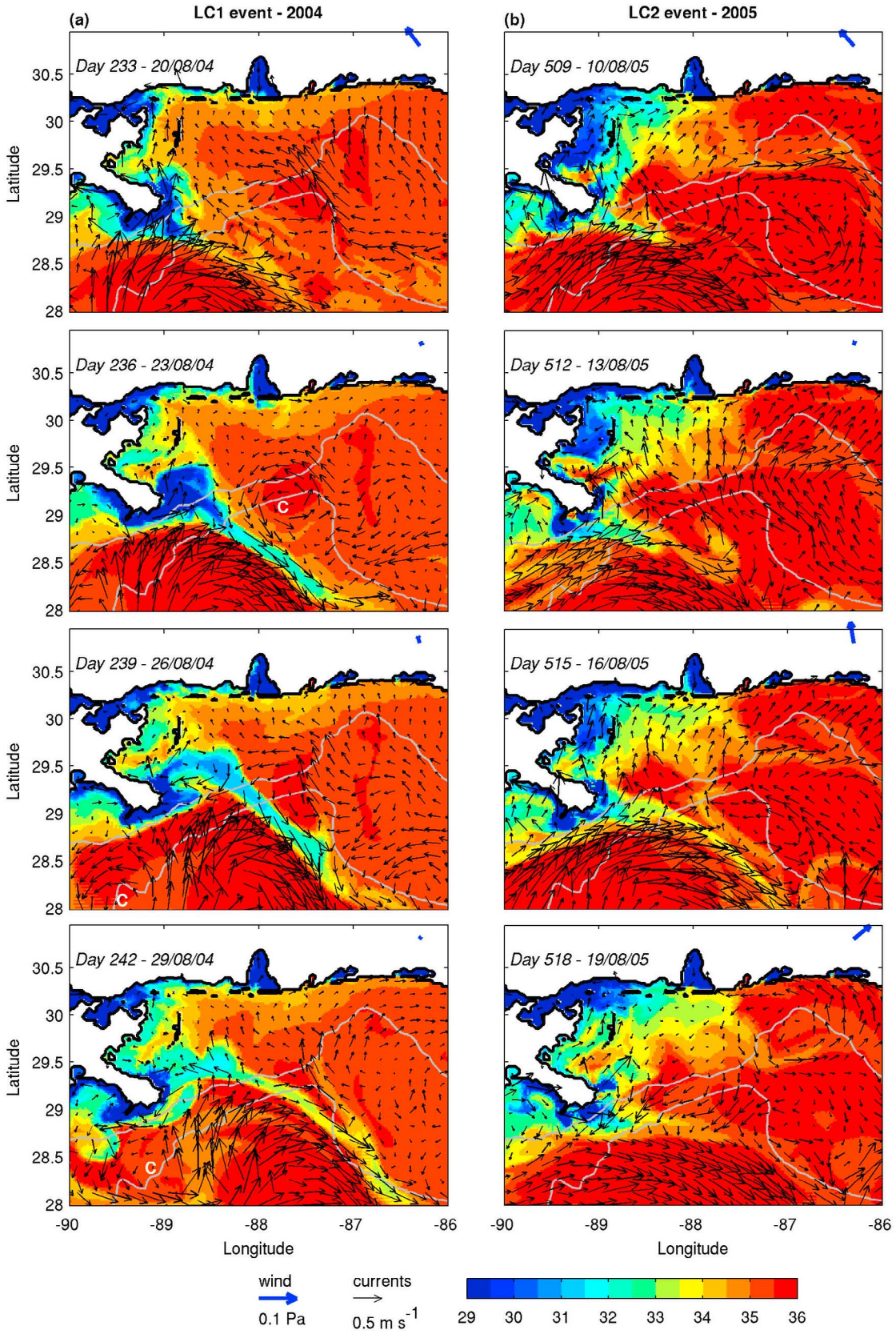

Figure 10. Same as Figure 9 but for LC periods (a) LC1 and (b) LC2.

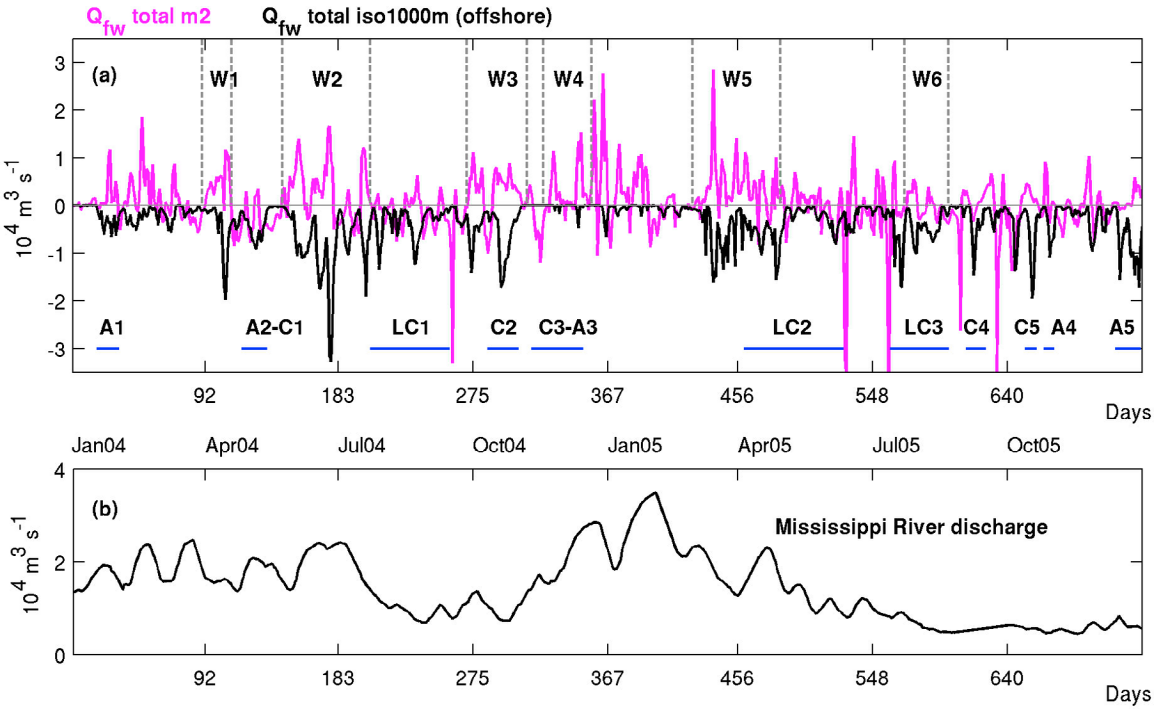

Figure 11. (a) Time series of total freshwater transport Q_{fw} across sections m2 and iso1000m (marked in Figure 3). Positive/negative values for eastward/westward transport across section m2. Only offshore (negative) portion of the transport is shown for the section iso1000m. Selected wind periods are delimited by vertical dashed gray lines. Periods of LC and eddy impacts are represented by horizontal blue lines. (b) Time series of Mississippi River discharge for the period of the simulation.

ods positively enhanced the offshore removal (W3 and C1, for example). The exception is period W4, when the three bursts of eastward transport were not followed by offshore removal. During that time, the eddy event C3-A3 negatively affected the transport of plume waters into the deep ocean (Figure 12a). The dipole circulation induced by the cyclone and the large anticyclone (~130 km in diameter) generated persistent onshore flows to the east of the MR delta for approximately 30 days. When the favorable wind period started, plume waters were advected eastward, caught in the anticyclonic circulation and transported toward the head of the DeSoto Canyon, where they were wrapped around the eddy. The eddy circulation has shifted the offshore pathway from the vicinity of the delta to head of the canyon.

[32] Although eastward, wind-driven transport of freshwater may initiate and promote the entrainment by the offshore circulation, offshore removal of plume waters is also observed during eddy events that are not favored by eastward transport. The best examples are during event LC1 and at the end of LC2, when the large anticyclonic circulation from the LC system dominated the offshore circulation south of the MR delta and captured the MR plume. Other eddy events of smaller scale also entrained the MR plume during wind conditions that did not favor offshore transport. During the eddy event A2-C1 (Figure 12b), winds were mostly from the southeast and that produced a westward plume transport toward the Louisiana-Texas shelf. However, the eddy dipole formed by the anticyclone A2 and the cyclone C1 (~50 km in diameter) was positioned just off of the MR delta, and the offshore currents generated by the eddy dipole were able to capture the MR plume even in the presence of southeasterly winds.

[33] Figure 11b shows a time series of the MR discharge during the period of simulation, and puts in perspective the offshore transport of plume waters with respect to the variability of the MR discharge. The transport of river waters to the interior of the gulf takes place throughout different stages of the MR outflow, during both flood and dry seasons. Continuous offshore removal happens during low-discharge conditions (events LC3 and beyond), whereas no removal takes place during high-discharge conditions (period W4 until the beginning of period W5). Based on the time series across iso1000m (Figure 11a), we computed the total volume of freshwater that was exported to the offshore region for each removal period (wind, LC and eddies) and compared with the freshwater volume discharge by the Mississippi River (Table 1). LC/eddy events that are superimposed with wind events by a few days are treated as a single (combined) exportation period. During the simulation period, the volume of freshwater removed to the offshore GoM ranged from approximately 5 km^3 to 43 km^3, with the largest volumes associated with wind events. Smaller volumes were associated with eddy events and the largest removal that was exclusively due to the offshore circulation happened during event LC1, when ~16 km^3 of freshwater were ejected offshore.

[34] The proximity of section iso1000m to the MR delta suggests that most of the freshwater exported across iso1000m is of MR origin. Table 1 shows the ratio of the volume of

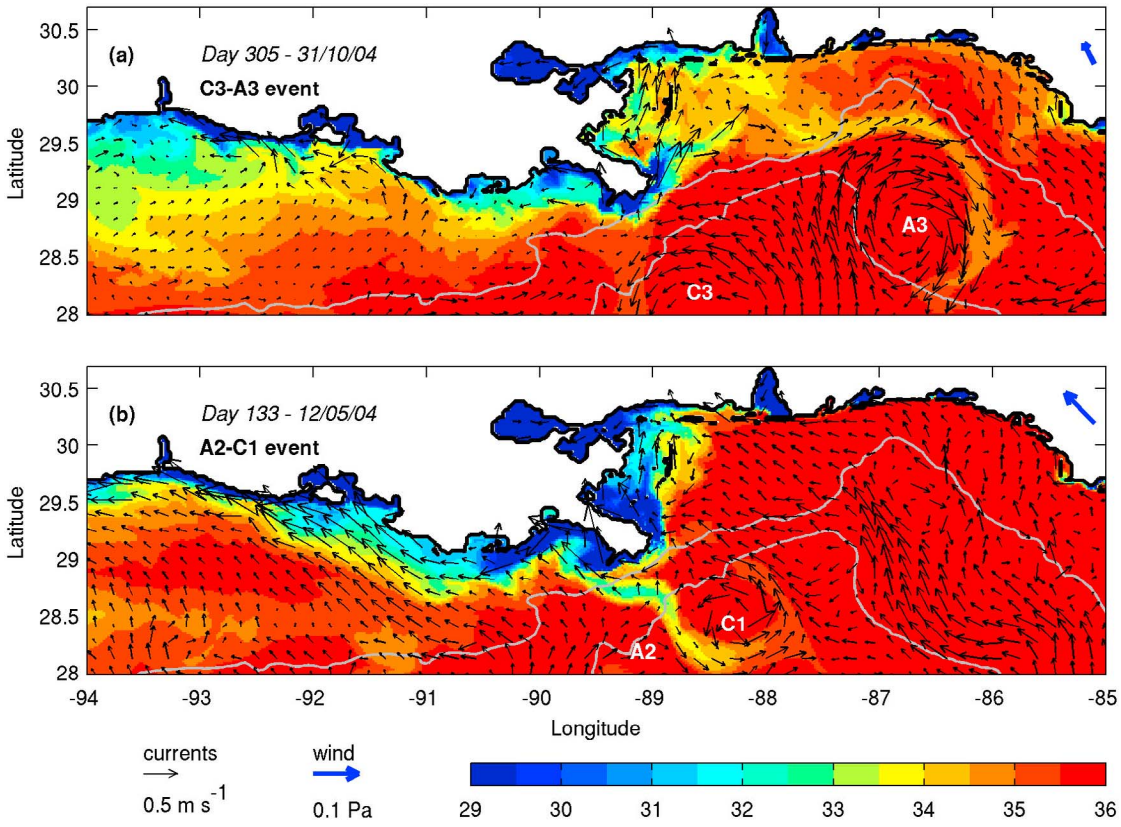

Figure 12. Snapshots of sea surface salinity and surface velocity vectors during two eddy events (a) C3-A3 and (b) A2-C1. Part of the model domain is shown. Vectors are shown every other eight grid points for better visualization. The gray lines represent the 100 and 1000 m isobaths. A and C show the location of anticyclonic and cyclonic eddies, respectively. For each day, the wind stress vector averaged over the area *A* is presented on the upper right corner. Salinity values less than 29 are not shown.

freshwater exported offshore to the ratio discharged by the Mississippi River. During the period of wind influence only (W2, no LC impact), winds promoted an offshore transport that corresponded to 40% of the MR discharge, while during the period of LC impact only (LC1, no wind contribution), the LC system captured a fraction corresponding to 35%. In the mixed forcing periods, the fractions corresponded to 28% (W5/LC2) and up to 78% (W6/LC3). In other eddy cases, ratios are larger than one and that suggests that pre-existent freshwater on the shelf break was also exported offshore. Although these estimates are simplified and not intended to be an accurate freshwater budget, they can be employed to elucidate the processes controlling the removal of MR waters away from the delta. In particular, our results show that offshore pathways are an active "sink" of plume waters and should be considered in conjunction with the shelf pathways of MR waters removal.

4.3.2. MR Plume Pathways Observed With Chlorophyll *a* Satellite Imagery

[35] We performed a qualitative comparison between the major wind (W2 and W5) and LC (LC1 and LC2) events from Figures 9 and 10 and chlorophyll *a* satellite images from the Indian Oceansat-1 Ocean Color Monitor (OCM). Satellite radiance measurements were used to track river water using ocean color channels with relatively high spatial resolutions of 360 m, compared with the Sea-viewing Wide

Table 1. Total Freshwater Volume Exported to the Offshore Region During Each Wind, Loop Current and Eddy Event[a]

Event	Duration (days)	Total Volume (km^3)	Volume Discharged by the MR (km^3)	Ratio Exported/Discharged
A1	16	4.94	24.90	0.19
W1	21	8.61	28.76	0.29
A2-C1	18	7.66	30.44	0.25
W2	61	43.21	106.12	0.40
LC1	55	16.26	45.31	0.35
W3/C2	42	18.49	37.61	0.49
W4/C3-A3	42	0.82	74.91	0.01
W5/LC2	104	39.63	140.48	0.28
W6/LC3	41	18.37	23.28	0.78
C4	14	5.04	6.55	0.76
C5	9	6.12	4.33	1.41
A4	8	3.52	3.33	1.05
A5	18	13.37	10.07	1.32

[a]W denotes a wind event, LC denotes a Loop Current event, A and C denote anticyclonic and cyclonic eddy events, respectively. Events that were superimposed in time are put together as one single exportation period (W5 and LC2, for example). The freshwater volume discharged by the Mississippi River during each period is also shown, together with the ratio between the volume exported and the volume discharged.

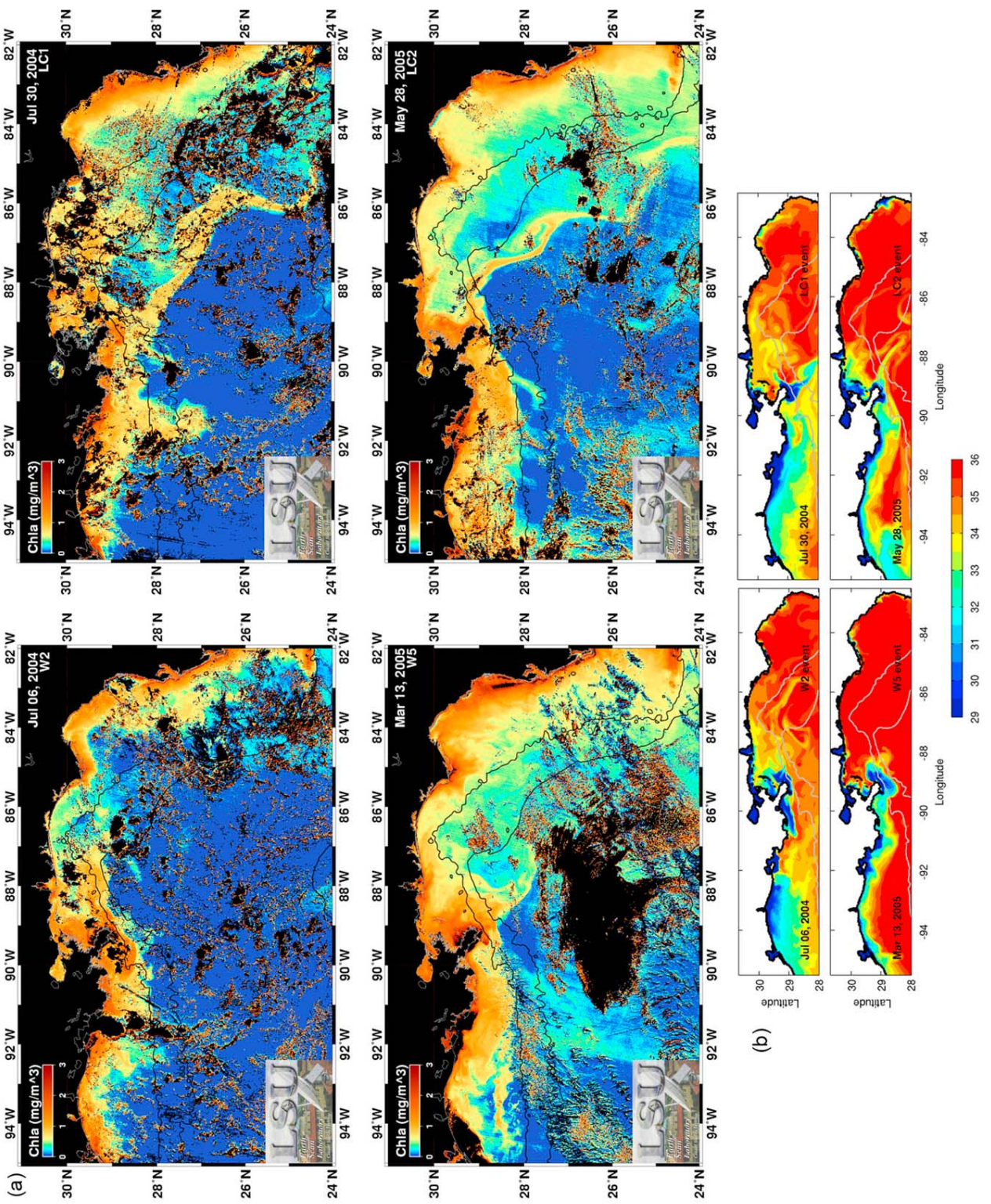
(a)
Jul 06, 2004
W2
Jul 30, 2004
LC1
Mar 13, 2005
W5
May 28, 2005
LC2
Chla (mg/m^3)
(b)
W2 event
LC1 event
W5 event
LC2 event
Jul 06, 2004
Jul 30, 2004
Mar 13, 2005
May 28, 2005
Latitude
Longitude

Figure 13

Field-of-View Sensor (SeaWiFS) that has 1.1 km pixels. The SeaSpace Terascan™ software, based on standard NASA algorithms for SeaWiFS [*Gordon and Wang*, 1994], was used to compute chlorophyll *a* using the 0.49 and 0.56 μm channels as input. Although these chlorophyll *a* estimates have not been validated for accuracy, they are effective for tracking the motion of near-surface, nutrient-rich river waters in the northern Gulf of Mexico, as previously described by *Walker et al.* [2005a].

[36] Figure 13a shows chlorophyll *a* images on specific days that represent the offshore removal of plume waters during the selected wind or LC event. Days were chosen based on the cloud coverage and availability of the image. Figure 13b shows the corresponding model surface salinity on the same days as the satellite images. The image on 6 July 2004 (model day 188) corresponds to a time at the end of period W2, when southerly winds favored the eastward transport of plume waters. A large signal of higher chlorophyll *a* concentration is observed to the east of the delta and over the shelf break. The signal extends into the interior of the DeSoto Canyon, and that suggests offshore removal by the mesoscale circulation. The image is in good qualitative agreement with the eastward transport and entrainment of plume waters described during event W2 (Figure 9a). The salinity distribution to the east of the delta on the same day (Figure 13b) shows the end product of the W2 period, when low-salinity waters of MR origin were transported in large volumes toward the DeSoto Canyon, then mixed and stirred by the offshore circulation. Similar agreement is observed on 13 March 2005 (model day 438), during the wind event W5. The chlorophyll *a* signal in the surroundings of the delta suggests an eastward transport of plume waters, in agreement with the model surface salinity on the same day. A pool of low-salinity waters is observed to the east of the MR delta, which is the initial stage of the eastward transport observed during wind event W5 (Figure 9b).

[37] The satellite images during the LC events demonstrate the remarkable impact of the LC system over the transport of the MR plume. On 30 July 2004 (model day 212, period LC1), a distinct chlorophyll *a* band extends from the MR delta into the interior of the GoM, reaching as south as 24°N. *Hu et al.* [2005] reported the same removal event and attributed it to the northward position of the LC, which is in agreement with the LC maximum latitude analysis (Figure 6) and the model results for period LC1. The model surface salinity on the same day (Figure 13b) is in good qualitative agreement and shows the corresponding low-salinity band, which extends from the MR delta into the offshore region and to the southern boundary of the NGoM-HYCOM model. The satellite image on 28 May 2005 (model day 514, event LC2) also reveals a distinct chlorophyll *a* band extending into the GoM, which agrees with the LC conditions during this period (Figure 6). The oligotrophic conditions on the west side of the band suggest that the riverine waters are being transported along the edge of the Loop Current. The model surface salinity on the same day shows the presence of the low-salinity band just to the east of the delta, in agreement with the position of the chlorophyll *a* band across the shelf break. The satisfactory comparison reinforces the necessity to employ a modeling approach that uses lateral boundary conditions from a realistic, data-assimilative ocean model, in order to capture strong interactions between the MR plume and the Loop Current.

5. Discussion

[38] The results presented in section 4 reveal the complex environmental conditions that control the evolution of the MR plume and the transport of the related low-salinity, nutrient-rich waters. The MR delta is located in a unique environment, where complex bottom topography, variable wind forcing and strong boundary currents actively impact the dynamics and the transport of the buoyant plume. This study presents a novel analysis of the combined effects of shelf and offshore flows in tandem with topographic controls, on the evolution of a large-scale river discharge.

[39] Previous observations [*Walker*, 1996; *Walker et al.*, 2005a] and numerical studies [*Wang and Justić*, 2009] have demonstrated the impact of different wind conditions over the structure of the MR plume. We studied the wind influence from the perspective of the plume freshwater transport, and our results are in agreement with previous observations and climatology-forced numerical modeling studies [*Morey et al.*, 2003a, *Walker et al.*, 2005a]. With respect to the along-shelf transport, the predominant transport pathway is to the west and toward the Louisiana-Texas shelf, due to prevalent easterly wind conditions in the region (Figure 5b). Easterly winds (southeasterly to northeasterly) predominate in the spring, autumn and winter months with an average annual frequency of 64% [*Walker and Hammack*, 2000], therefore making the Louisiana-Texas shelf the most frequent MR plume pathway. Large eastward transport is observed when persistent southerly southwesterly winds develop, such as toward the end of the spring and during summer months (Figure 5c). During that time, the plume circulation can be completely reversed and riverine waters are dispersed to the east of the delta with a small fraction toward the north, and that process significantly impacts the distribution of low-salinity waters in the region. Westerly winds in the winter and in the fall also induce eastward transport, but they are much shorter in duration, because they are associated with the passage of cold fronts and not with a change in the seasonal pattern of the wind field. Furthermore, estimates of across-shelf freshwater transport in the vicinity of the delta demonstrate that the offshore transport can be as large as the along-shelf transport (Figure 5e). The proximity of the shelf break to the freshwater source allows the MR plume to be constantly expanded offshore and transported on and off the shelf, and the large variability in the cross-isobath transport

Figure 13. (a) Oceansat-1 OCM chlorophyll *a* images from selected days during events W2, W5, LC1 and LC2. The chlorophyll *a* scale ranges from 0 to 3 mg m^{-3}. The 100 and 1000 m isobaths are shown as black lines. River water is depicted in red/brown tones near the mouth of rivers, where pigment concentrations are highest and orange/yellow tones in deep water, where pigment concentrations are reduced. (b) Snapshots of model sea surface salinity on the same days as the satellite images. The 100 and 1000 m isobaths are displayed as gray lines. Salinity values less than 29 are not shown.

near the delta suggests that changes in the wind direction are important for the offshore removal close to the source.

[40] If in the vicinity of the delta the steep bottom topography favors the offshore transport of plume waters, the broadening of the shelf to the west of the delta maintains the plume away from the shelf break and "insulated" from the offshore circulation. To the east of the delta, the presence of the DeSoto Canyon facilitates the interactions of the plume with the offshore circulation when the plume is transported eastward, specially in the presence of southerly/southwesterly winds. Under those wind conditions, offshore eddies effectively entrain the plume as low-salinity bands that are subsequently strained and dispersed by the mesoscale circulation (Figure 9). Although this process was previously discussed by *Morey et al.* [2003a, 2003b], our simulations allowed estimates of freshwater transport, which showed a new result: large volumes of freshwater can be ejected offshore through shelf to deep current interactions. Volumes as large as $40km^3$ were removed by the mesoscale circulation during prolonged periods of winds that transport the plume eastward (Table 1). One characteristic of the eddy removal during periods of eastward transport is that after the plume is entrained, it is "locally" mixed and dispersed in the region of the DeSoto Canyon. When the plume is directly entrained by offshore eddies, especially by the LC system, coherent low-salinity bands extend from the delta to the southern boundary of the NGoM-HYCOM domain, and are erased just after the passage of the eddy circulation. This distinction suggests that the isolated impact of mesoscale eddies maybe more efficient in transporting plume waters further offshore and into the interior of the GoM.

[41] In situ measurements of salinity for the quantitative evaluation of the plume surface salinity fields were not available for the study period. We performed a qualitative comparison between the modeled plume and chlorophyll *a* satellite images during selected events of plume transport. The position and extent of the modeled low-salinity plume was in good agreement with the satellite high-chlorophyll plume signal, which indicates the good performance of the model with respect to the timing and extent of the transport events. Chlorophyll *a* satellite imagery has been used as a qualitative proxy to river induced salinity fronts in several modeling and observational studies [*McClain et al.*, 1988; *Kourafalou et al.*, 1996b; *Tsiaras et al.*, 2008; *Hickey et al.*, 2010]. In particular, the Mississippi River plume has been tracked using satellite measurements of reflectance [*Walker et al.*, 1994, 2005a; *Walker*, 1996; *Green et al.*, 2006; *Hu et al.*, 2005] and using chlorophyll *a* estimates [*Walker et al.*, 2005a, 2005b; *Hu et al.*, 2004].

[42] Observational studies [*Walker et al.*, 1994; *Ortner et al.*, 1995; *Gilbert et al.*, 1996; *Hu et al.*, 2005] have described transport pathways of MR waters along the Loop Current and toward the Florida Current and the Gulf Stream, but lacked information about the physical processes that initiated this unique cross-marginal removal mechanism in the NGoM region. In this study, we elucidated the specific entrainment process at the freshwater source, and showed how the intrusion of the LC system was an effective mechanism for the offshore transport of plume waters (Figure 10). The entrainment by the LC happened regardless of the wind field, as the proximity of the LC to the MR delta was a sufficient condition to capture the plume. Other eddies located in the vicinity of the shelf break with diameters ranging from 50 to 130 km also played important roles as sinks of riverine waters. Slope eddies [*Hamilton et al.*, 2002; *Hamilton and Lee*, 2005] actively entrained plume waters, and the formation of anticyclone-cyclone pairs generated offshore-directed currents that were capable of entraining plume waters even in the presence of southeasterly winds (Figure 12b). Conversely, cyclone-anticyclone pairs generated onshore currents that blocked wind-induced tendency for offshore removal of plume waters. In such cases, plume waters were advected toward the head of the DeSoto Canyon (Figure 12a). Similar interactions between the MR plume and large anticyclones were observed before [*Walker et al.*, 1996, 2005a; *Muller-Karger*, 2000]. Our results demonstrate that the positioning and proximity of eddies to the shelf break strongly determines the characteristics of the offshore freshwater transport and imposes a large variability in the offshore pathways that the plume may take.

[43] Hypoxia conditions on the Louisiana-Texas shelf in the summer time have been attributed to the discharge of the Mississippi/Atchafalaya River System, and a combination of biological and physical factors [*Justić et al.*, 2007]. Inner shelf currents transport riverine waters to the Louisiana-Texas shelf, where the nutrient-rich freshwater enhances the surface biological productivity and consequently the carbon flux to sediments. This process creates a subsurface layer where bacterial decomposition of organic matter and oxygen consumption are high. At the same time, the freshwater and weak wind conditions in the summer enhance the water column vertical stratification, which decreases the flux of oxygen from the atmosphere to the bottom layers. Ultimately, the combination of these processes leads to the formation of subsurface layers where oxygen concentrations are extremely low, with adverse conditions for marine organisms. Preceding three-dimensional numerical modeling studies have focused on the transport and circulation of the MR plume waters to the west of the delta, with emphasis on the physical aspects that promote the development of hypoxia conditions [*Hetland and DiMarco*, 2008; *Wang and Justić*, 2009]. In spite of the advancement in the knowledge of the physical processes related to hypoxia, these modeling studies lacked the implementation of lateral boundary conditions that incorporate the effects of the LC dynamics and offshore eddies. Our results demonstrate that mesoscale eddies can play an important role on the cross-marginal transport of the nutrient-rich, low-salinity waters. The alongshore pathways are thus also influenced, since such eddy events reduce the transport of riverine waters to the Louisiana-Texas shelf, with possible implications on the local development of hypoxia. Our results showed that entrainment can happen year-round, and that the time scale of these events range from weeks to months (Table 1). *Hamilton and Lee* [2005] observed that the dominant eddies in the northern GoM can have time scales on the order of 100 days, which suggests that the eddies can interact with the MR plume for a long time if they are well positioned in the vicinity of the delta. Future studies employing realistically forced simulations that are integrated for several years should provide a broader and clearer picture of the relative importance of mesoscale eddies to the dynamics and pathways of the MR

plume, to the freshwater budget of the NGoM region and to the hypoxia problem on the Louisiana-Texas shelf.

6. Concluding Remarks

[44] A high-resolution numerical model of the NGoM region was developed and employed in a realistically forced experiment to investigate the dynamics of the MR plume, and the impact of the wind-driven and eddy-driven dynamics on the fate of riverine waters. Emphasis was given to the processes responsible for the across-shelf transport of the plume, and the conditions that favor the offshore exportation of the MR waters. The results presented herein demonstrate that both wind-driven and eddy-driven dynamics play major roles in the transport and dispersion of the MR plume, and that the bottom topography in the NGoM region is a determinant factor in the offshore removal of plume waters. Along-shelf freshwater transport was strongly related to wind-driven, shelf currents. The prevailing easterly winds throughout the year transport plume waters toward the Louisiana-Texas shelf, where broadening of the shelf reduces the interactions between the plume and the offshore eddy field. Short-term wind reversals in the fall and winter may transport the plume to the east, where the shelf is narrow and interactions between the plume and eddies are facilitated. However, our simulation suggests that these reversals are generally too short to enable an efficient entrainment by eddies. The offshore removal of the plume is maximized when the winds are predominantly from the south–southwest. During those wind periods, large portions of MR waters are advected eastward along the rim of the DeSoto Canyon, where the plume can be easily entrained by the mesoscale field.

[45] An important finding is that offshore removal by eddies does not exclusively happen during winds that favor offshore transport. The complex topography of the shelf areas around the MR plume plays a role in the offshore transport of plume waters, which can thus occur even in the presence of opposing winds. The proximity of mesoscale eddies to the head of the Delta is a sufficient condition to entrain the plume. During entrainment events, the size and position of the eddies, as well as the formation of eddy pairs, determine a variety of offshore pathways of the MR plume. The offshore transport by eddies can be as large as the along-shelf transport, and this result demonstrates that the offshore eddy field is an active component of the plume dynamics. We conclude that the Loop Current System is an energetic pathway for the offshore transport of riverine waters. In addition, the variability of the Loop Current front and the associated eddy field are found to be a major dynamical factor in the connectivity between the northern Gulf of Mexico and the basin interior. This finding has a variety of environmental implications, associated with the transport of low-salinity waters, but also nutrients and pollutants. The latter has been evident in the recent Deepwater Horizon oil spill incident (22 April 2010), where the surface oil slick has been observed around the MR plume, but also removed from the northern gulf and toward the interior by the surrounding eddy field.

[46] This study highlights that in order to obtain a complete picture of the processes determining the fate of large buoyant outflows in topographically complex marginal seas, it is necessary to downscale larger-scale coarser models, and to employ a nesting approach to properly reproduce complex interactions between the coastal and offshore circulation patterns. Nesting to a data assimilative model, as performed herein, is a desirable approach to ensure proper shelf to offshore interactions. The findings from this study can be employed for the understanding of plume dynamics in the presence of energetic boundary flows in general, and for the design of an integrated observational and modeling system over the northern Gulf of Mexico, in particular.

[47] **Acknowledgments.** The study was funded by the National Science Foundation (NSF OCE-0929651) and the National Oceanic and Atmospheric Administration (NOAA NA17RJ1226). Additional funding for V. H. Kourafalou and P. Hogan was available from the Office of Naval Research through the National Ocean Partnership Program (ONR/NOPP N000140510892). The authors are very thankful to Richard Patchen (NOAA National Ocean Service) for providing the realistic river discharge data set employed in this study, to Robert Leben (University of Colorado) for providing the Loop Current tracking program that was used in the analysis of model results and to Chet Pilley (Earth Scan Laboratory, Louisiana State University) for his assistance with satellite image processing.

References

Bleck, R. (2002), An oceanic circulation model framed in hybrid isopycnic-Cartesian coordinates, *Ocean Modell.*, *4*, 55–88, doi:10.1016/S1463-5003(01)00012-9.

Browning, G. L., and H.-O. Kreiss (1982), Initialization of the shallow water equations with open boundaries by the bounded derivative method, *Tellus*, *34*, 334–351, doi:10.1111/j.2153-3490.1982.tb01823.x.

Browning, G. L., and H.-O. Kreiss (1986), Scaling and computation of smooth atmospheric boundary conditions, *Tellus A*, *38*, 295–313.

Chao, S. Y. (1988), Wind-driven motion of estuarine plumes, *J. Phys. Oceanogr.*, *18*, 1144–1166, doi:10.1175/1520-0485(1988)018<1144:WDMOEP>2.0.CO;2.

Chassignet, E. P., L. T. Smith, and G. R. Halliwell (2003), North Atlantic simulations with the Hybrid Coordinate Ocean Model (HYCOM): Impact of the vertical coordinate choice, reference pressure and thermobaricity, *J. Phys. Oceanogr.*, *33*, 2504–2526, doi:10.1175/1520-0485(2003)033<2504:NASWTH>2.0.CO;2.

Chérubin, L. M., Y. Morel, and E. P. Chassignet (2006), Loop Current ring shedding: The formation of cyclones and the effect of topography, *J. Phys. Oceanogr.*, *36*, 569–591, doi:10.1175/JPO2871.1.

Cochrane, J. D., and F. J. Kelly (1986), Low-frequency circulation on the Texas-Louisiana continental shelf, *J. Geophys. Res.*, *91*, 10,645–10,659, doi:10.1029/JC091iC09p10645.

Csanady, G. T. (1978), The arrested topographic wave, *J. Phys. Oceanogr.*, *8*, 47–62, doi:10.1175/1520-0485(1978)008<0047:TATW>2.0.CO;2.

Cummings, J. A. (2005), Operational multivariate ocean data assimilation, *Q. J. R. Meteorol. Soc.*, *131*, 3583–3604, doi:10.1256/qj.05.105.

Fong, D. A., and W. R. Geyer (2001), Response of a river plume during an upwelling favorable wind event, *J. Geophys. Res.*, *106*, 1067–1084, doi:10.1029/2000JC900134.

Fratantoni, P. S., T. N. Lee, G. P. Podestá, and F. Muller-Karger (1998), The influence of Loop Current perturbations on the formation and evolution of Tortugas eddies in the southern Straits of Florida, *J. Geophys. Res.*, *103*, 24,759–24,779, doi:10.1029/98JC02147.

Gilbert, P. S., T. N. Lee, and G. P. Podestá (1996), Transport of anomalous low-salinity waters from the Mississippi River flood of 1993 to the Straits of Florida, *Cont. Shelf Res.*, *16*, 1065–1085, doi:10.1016/0278-4343(95)00056-9.

Gordon, H. R., and M. Wang (1994), Retrieval of water leaving radiance and aerosol optical thickness over the oceans with SeaWiFS: A preliminary algorithm, *Appl. Opt.*, *33*, 443–452, doi:10.1364/AO.33.000443.

Green, R. E., T. S. Bianchi, M. J. Dagg, N. D. Walker, and G. A. Breed (2006), An organic carbon budget for the Mississippi River turbidity plume and plume contributions to air-sea CO_2 fluxes and bottom water hypoxia, *Estuaries Coasts*, *29*, 579–597.

Halliwell, G. R. (2004), Evaluation of vertical coordinate and vertical mixing algorithms in the Hybrid-Coordinate Ocean Model (HYCOM), *Ocean Modell.*, *7*, 285–322, doi:10.1016/j.ocemod.2003.10.002.

Halliwell, G. R., A. Barth, R. H. Weisberg, P. Hogan, O. M. Smedstad, and J. Cummings (2009), Impact of GODAE products on nested HYCOM

simulations of the west Florida shelf, *Ocean Dyn.*, *59*, 139–155, doi:10.1007/s10236-008-0173-2.

Hamilton, P., and T. N. Lee (2005), Eddies and jets over the slope of the northeast Gulf of Mexico, in *Circulation of the Gulf of Mexico: Observations and Models*, *Geophys. Monogr. Ser.*, vol. 161, edited by W. Sturges and A. Lugo-Fernandes, pp. 123–142, AGU, Washington, D. C.

Hamilton, P., T. J. Berger, and W. Johnson (2002), On the structure and motions of cyclones in the northern Gulf of Mexico, *J. Geophys. Res.*, *107*(C12), 3208, doi:10.1029/1999JC000270.

Hetland, R. D., and S. F. DiMarco (2008), How does the character of oxygen demand control the structure of hypoxia on the Texas-Louisiana continental shelf?, *J. Mar. Syst.*, *70*, 49–62, doi:10.1016/j.jmarsys.2007.03.002.

Hickey, B. M., et al. (2010), River influences on shelf ecosystems: Introduction and synthesis, *J. Geophys. Res.*, *115*, C00B17, doi:10.1029/2009JC005452.

Hodur, R. M., J. Pullen, J. Cummings, X. Hong, D. Doyle, P. J. Martin, and M. A. Rennick (2002), The Coupled Ocean/Atmospheric Mesoscale Prediction System (COAMPS), *Oceanography*, *15*, 88–98.

Hu, C., B. Nababan, D. C. Biggs, and F. E. Muller-Karger (2004), Variability of bio-optical properties at sampling stations and implications for remote sensing: A case study in the north-east Gulf of Mexico, *Int. J. Remote Sens.*, *25*, 2111–2120, doi:10.1080/01431160310001618789.

Hu, C., J. R. Nelson, E. Johns, Z. Chen, R. H. Weisberg, and F. E. Muller-Karger (2005), Mississippi River water in the Florida Straits and in the Gulf Stream off Georgia in summer 2004, *Geophys. Res. Lett.*, *32*, L14606, doi:10.1029/2005GL022942.

Huh, O. K., W. J. Wiseman Jr., and L. J. Rouse Jr. (1981), Intrusion of Loop Current waters onto the west Florida continental shelf, *J. Geophys. Res.*, *86*, 4186–4192, doi:10.1029/JC086iC05p04186.

Hurlburt, H. E., and J. D. Thompson (1980), A numerical study of Loop Current intrusions and eddy shedding, *J. Phys. Oceanogr.*, *10*, 1611–1651, doi:10.1175/1520-0485(1980)010<1611:ANSOLC>2.0.CO;2.

Justić, D., J. V. Bierman, D. Scavia, and D. R. Hetland (2007), Forecasting gulf's hypoxia: The next 30 years?, *Estuaries Coasts*, *30*, 791–801.

Kara, A. B., H. E. Hurlburt, and A. J. Wallcraft (2005), Stability-dependent exchange coefficients for air-sea fluxes, *J. Atmos. Oceanic Technol.*, *22*, 1080–1094, doi:10.1175/JTECH1747.1.

Kourafalou, V. H., L.-Y. Oey, J. Wang, and T. N. Lee (1996a), The fate of river discharge on the continental shelf: 1. Modeling the river plume and the inner shelf coastal current, *J. Geophys. Res.*, *101*, 3415–3434, doi:10.1029/95JC03024.

Kourafalou, V. H., T. N. Lee, L.-Y. Oey, and J. D. Wang (1996b), The fate of river discharge on the continental shelf: 2. Transport of coastal low-salinity waters under realistic wind and tidal forcing, *J. Geophys. Res.*, *101*, 3435–3455, doi:10.1029/95JC03025.

Kourafalou, V. H., G. Peng, H. Kang, P. J. Hogan, O. M. Smedstad, and R. H. Weisberg (2009), Evaluation of Global Ocean Data Assimilation Experiment products on south Florida nested simulations with the Hybrid Coordinate Ocean Model, *Ocean Dyn.*, *59*, 47–66, doi:10.1007/s10236-008-0160-7.

Large, W. G., J. C. McWilliams, and S. C. Doney (1994), Oceanic vertical mixing: A review and a model with a nonlocal boundary layer parameterization, *Rev. Geophys.*, *32*, 363–403, doi:10.1029/94RG01872.

Leben, R. R. (2005), Altimetry-derived Loop Current metrics, in *Circulation of the Gulf of Mexico: Observations and Models*, *Geophys. Monogr. Ser.*, vol. 161, edited by W. Sturges and A. Lugo-Fernandes, pp. 181–201, AGU, Washington, D. C.

Li, Y., W. D. Nowlin Jr., and R. O. Reid (1997), Mean hydrographic fields and their interannual variability over the Texas-Louisiana continental shelf in spring, summer and fall, *J. Geophys. Res.*, *102*, 1027–1049, doi:10.1029/96JC03210.

Maul, G. H. (1977), The annual cycle of the gulf Loop Current Part, part I: Observations during a one-year time series, *J. Mar. Res.*, *33*, 29–47.

McClain, C. R., J. A. Yoder, L. P. Atkinson, J. O. Blanton, T. N. Lee, J. J. Singer, and F. Muller-Karger (1988), Variability of surface pigment concentrations in the South Atlantic Bight, *J. Geophys. Res.*, *93*, 10,675–10,697, doi:10.1029/JC093iC09p10675.

Milliman, J. D., and R. H. Meade (1983), World-wide delivery of river sediment to the ocean, *J. Geol.*, *91*, 1–21, doi:10.1086/628741.

Morey, S. L., P. J. Martin, J. J. O'Brien, A. A. Wallcraft, and J. Zavala-Hidalgo (2003a), Export pathways for river discharged fresh water in the northern Gulf of Mexico, *J. Geophys. Res.*, *108*(C10), 3303, doi:10.1029/2002JC001674.

Morey, S. L., W. W. Schroeder, J. J. O'Brien, and J. Zavala-Hidalgo (2003b), The annual cycle of riverine influence in the eastern Gulf of Mexico basin, *Geophys. Res. Lett.*, *30*(16), 1867, doi:10.1029/2003GL017348.

Muller-Karger, F. E. (2000), The spring 1998 northeastern Gulf of Mexico (NEGOM) cold water event: Remote sensing evidence for upwelling and for eastward advection of Mississippi water (or: How and errant Loop Current anticyclone took the NEGOM for a spin), *Gulf Mex. Sci.*, *1*, 55–67.

Nowlin, W. D., Jr., A. E. Jochens, M. K. Howard, S. F. DiMarco, and W. W. Schroeder (2000), Hydrographic properties and inferred circulation over the northeastern shelves of the Gulf of Mexico during spring to midsummer of 1998, *Gulf Mex. Sci.*, *1*, 40–54.

Nowlin, W. D., Jr., A. E. Jochens, and S. F. DiMarco (2005), Low-frequency circulation over the Texas-Louisiana continental shelf, in *Circulation of the Gulf of Mexico: Observations and Models*, *Geophys. Monogr. Ser.*, vol. 161, edited by W. Sturges and A. Lugo-Fernandes, pp. 219–240, AGU, Washington, D. C.

Ohlmann, J. C., P. P. Niiler, C. A. Fox, and R. B. Leben (2001), Eddy energy and shelf interactions in the Gulf of Mexico, *J. Geophys. Res.*, *106*, 2605–2620, doi:10.1029/1999JC000162.

Ortner, P. B., T. N. Lee, P. J. Milne, R. G. Zika, M. E. Clarke, G. P. Podestá, P. K. Swart, P. A. Tester, L. P. Atkinson, and W. R. Johnson (1995), Mississippi River flood waters that reached the Gulf Stream, *J. Geophys. Res.*, *100*, 13,595–13,601, doi:10.1029/95JC01039.

Paluszkiewicz, T., L. P. Atkinson, E. S. Posmentier, and C. R. McClain (1983), Observation of a Loop Current frontal eddy intrusion onto the west Florida shelf, *J. Geophys. Res.*, *88*, 9639–9651, doi:10.1029/JC088iC14p09639.

Prasad, T. G., and P. J. Hogan (2007), Upper-ocean response to Hurricane Ivan in a 1/25° nested Gulf of Mexico HYCOM, *J. Geophys. Res.*, *112*, C04013, doi:10.1029/2006JC003695.

Rabalais, N. N., R. E. Turner, W. J. Wiseman Jr., and D. F. Boesh (1991), A brief summary of hypoxia on the northern Gulf of Mexico continental shelf: 1985–1988, in *Modern and Ancient Continental Shelf Anoxia*, *Spec. Publ. Ser.*, vol. 58, edited by R. V. Tyson and T. H. Pearson, pp. 35–47, Geol. Soc. of London, London.

Rabalais, N. N., R. E. Turner, and W. J. Wiseman Jr. (2002), Gulf of Mexico hypoxia, a.k.a. "the dead zone," *Annu. Rev. Ecol. Syst.*, *33*, 235–263, doi:10.1146/annurev.ecolsys.33.010802.150513.

Rabalais, N. N., R. E. Turner, B. K. Sen Gupta, D. F. Boesh, P. Chapman, and M. C. Murrell (2007), Hypoxia in the northern Gulf of Mexico: Does the science support the plan to reduce, mitigate, and control hypoxia?, *Estuaries Coasts*, *30*, 753–772.

Schiller, R. V., and V. H. Kourafalou (2010), Modeling river plume dynamics with the Hybrid Coordinate Ocean Model, *Ocean Modell.*, *33*, 101–117, doi:10.1016/j.ocemod.2009.12.005.

Schroeder, W. W., S. P. Dinnel, W. J. Wiseman Jr., and W. J. Merrell Jr. (1987), Circulation patterns inferred from the movement of detached buoys in the eastern Gulf of Mexico, *Cont. Shelf Res.*, *7*, 883–894, doi:10.1016/0278-4343(87)90004-5.

Stone, G. W., N. D. Walker, S. A. Hsu, A. Babin, B. Liu, B. D. Keim, W. Teague, D. Mitchell, and R. Leben (2005), Hurricane Ivan's impact along the northern Gulf of Mexico, *Eos Trans. AGU*, *86*(48), 497, 500–501, doi:10.1029/2005EO480001.

Sturges, W., and R. Leben (2000), Frequency of ring separations from the Loop Current in the Gulf of Mexico: A revised estimate, *J. Phys. Oceanogr.*, *30*, 1814–1819, doi:10.1175/1520-0485(2000)030<1814:FORSFT>2.0.CO;2.

Teague, W. J., E. Jarosz, M. R. Carners, D. A. Mitchell, and P. J. Hogan (2006), Low-frequency current variability observed at the shelfbreak in the northeastern Gulf of Mexico: May–October, 2004, *Cont. Shelf Res.*, *26*, 2559–2582, doi:10.1016/j.csr.2006.08.002.

Tsiaras, K., V. H. Kourafalou, A. Davidov, and J. Staneva (2008), A three-dimensional coupled model of the western Black Sea plankton dynamics: Seasonal variability and comparison to SeaWiFs data, *J. Geophys. Res.*, *113*, C07007, doi:10.1029/2006JC003959.

Vukovich, F. M. (1986), Aspects of the behavior of cold perturbations in the eastern Gulf of Mexico: A case study, *J. Phys. Oceanogr.*, *16*, 175–188, doi:10.1175/1520-0485(1986)016<0175:AOTBOC>2.0.CO;2.

Vukovich, F. M., B. W. Crissman, M. Bushnell, and W. J. King (1979), Some aspects of the oceanography of the Gulf of Mexico using satellite and in situ data, *J. Geophys. Res.*, *84*, 7749–7768, doi:10.1029/JC084iC12p07749.

Walker, N. D. (1996), Satellite assessment of Mississippi River plume variability: Causes and predictabiliy, *Remote Sens. Environ.*, *58*, 21–35, doi:10.1016/0034-4257(95)00259-6.

Walker, N. D., and A. B. Hammack (2000), Impacts of winter storms on circulation and sediment transport: Atchafalaya-Vermilion Bay region, Louisiana, U.S.A., *J. Coastal Res.*, *16*, 996–1010.

Walker, N. D., G. Fargion, L. J. Rouse Jr., and D. Biggs (1994), Circulation of Mississippi River water discharged into the northern Gulf of Mexico

by the great flood of summer 1993, *Eos Trans. AGU*, *75*(36), 409, 414–415, doi:10.1029/94EO01045.

Walker, N. D., O. K. Huh, L. J. Rouse Jr., and S. P. Murray (1996), Evolution and structure of a coastal squirt off the Mississippi River delta: Northern Gulf of Mexico, *J. Geophys. Res.*, *101*, 20,643–20,655, doi:10.1029/96JC00919.

Walker, N. D., S. Myint, A. Babin, and A. Hagg (2003), Advances in satellite radiometry for the surveillance of surface temperatures, ocean eddies and upwelling processes in the Gulf of Mexico using GOES-8 measurements during summer, *Geophys. Res. Lett.*, *30*(16), 1854, doi:10.1029/2003GL017555.

Walker, N. D., W. J. Wiseman Jr., L. J. Rouse Jr., and A. Babin (2005a), Effects of river discharge, wind stress, and slope eddies on circulation and satellite-observed structure of the Mississippi River plume, *J. Coastal Res.*, *216*, 1228–1244, doi:10.2112/04-0347.1.

Walker, N. D., R. R. Leben, and S. Balasubramanian (2005b), Hurricane-forced upwelling and chlorophyll a enhancement within cold-core cyclones in the Gulf of Mexico, *Geophys. Res. Lett.*, *32*, L18610, doi:10.1029/2005GL023716.

Wang, L., and D. Justić (2009), A modeling study of the physical processes affecting the development of seasonal hypoxia over the inner Louisiana-Texas shelf: Circulation and stratification, *Cont. Shelf Res.*, *29*, 1464–1476, doi:10.1016/j.csr.2009.03.014.

Wright, L. D., and J. M. Coleman (1971), Effluent expansion and interfacial mixing in the presence of a salt wedge, Mississippi River delta, *J. Geophys. Res.*, *76*, 8649–8661, doi:10.1029/JC076i036p08649.

Yuan, J., R. L. Miller, R. T. Powell, and M. J. Dagg (2004), Storm-induced injection of the Mississippi River plume into the open Gulf of Mexico, *Geophys. Res. Lett.*, *31*, L09312, doi:10.1029/2003GL019335.

P. Hogan, Naval Research Laboratory, Stennis Space Center, MS 39529, USA.

V. H. Kourafalou and R. V. Schiller, Rosenstiel School of Marine and Atmospheric Science, University of Miami, 4600 Rickenbacker Cswy., Miami, FL 33149, USA. (rschiller@rsmas.miami.edu)

N. D. Walker, Department of Oceanography and Coastal Sciences, Louisiana State University, 1002-Y Energy, Coast & Environment Bldg., Baton Rouge, LA 70803, USA.